



Carbon Nanomembranes

In situ cross-linking of SAMs by low-energy electrons

Thesis

submitted in partial fulfilment of the
requirements for the degree of

Bachelor of Science
in
Physics

Author:

Thomas de Beer

Student ID:

s1289667

Supervisor:

Dr. ir. S.J. van der Molen

2nd corrector:

Prof. dr. J.M. van Ruitenbeek

Leiden, The Netherlands, August 19, 2015

Table of contents

Table of contents.....	2
Abstract.....	3
1. Introduction	4
2. Methods	6
2.1 Sample preparation.....	6
2.2 SAM characterisation: Conducting probe atomic force microscopy.....	7
2.3 Low Energy Electron Microscopy	10
3. Results.....	13
3.1 SAM preparation	13
3.2 Testing UV light on BPT SAMs.....	13
3.3 Electron irradiation induced effect on BPT SAM	15
3.4 Structural investigation of the front.....	16
3.5 Front quality/visibility	17
3.6 'Frozen' front	18
3.7 Detailed analysis of front speed	20
3.8 Developing illuminated SAMs	22
4. Discussion	26
4.1 SAM results	26
4.2 Front interpretation & energy-dose	27
4.3 Possibly made CNM.....	29
5. Conclusion	30
6. Outlook	31
Acknowledgements.....	33
Appendix A.....	34
Appendix B	36
Reference list.....	38

Abstract

Carbon Nanomembranes (CNMs) are two-dimensional materials made by *cross-linking* (interconnecting) the molecules of a Self Assembled Monolayer (SAM). CNMs can be chemically tailored on one or both sides leading to a variety of possible properties (e.g. mechanical, conductive, chemical, etc.). Once these properties are understood and controlled, CNMs might be a candidate for (among other things) *functional* devices based on molecules. In this thesis, it is described how to create laterally patterned CNMs by cross-linking aromatic based self assembled monolayers. Cross-linking is done by *in situ* low-energy electron irradiation with low energy electron microscopy (LEEM). This novel method allows for new types of experiments giving a brand new perspective. We show that a new structure (possibly CNM) was created after electron irradiation of SAM followed by annealing, furthermore, we have learned that our SAMs show an electron irradiation induced effect. This effect is most accurately described as a front shaped like the irradiated area, slowly shrinking in size until its disappearance. This effect was observed right after irradiation if certain conditions on the illumination time and electron energy were met. This phenomenon was imaged live and down to micrometer scale. These measurements have brought us to the conclusion that this front is not shrinking with a constant speed but is accelerating just before its disappearance. Furthermore, our measurements hint for a connection between the parameters illumination time & electron energy and the visibility and speed of a front.

1. Introduction

For a long time, it was thought that stable, truly two-dimensional materials could not existⁱ. Thus the discovery of graphene¹ (flat, hexagonally arranged carbon atoms), excited scientists all over the world. Its monoatomic thickness was considered to be truly two-dimensional. Graphene has all sorts of interesting properties² (e.g. semiconductive with zero gap and linear dispersion, extremely light yet stronger than diamond³, etc). Lately, a new (nearly) two-dimensional structure has drawn a lot of interest: Carbon Nanomembranes (CNMs). They are slightly thicker (~ 1 nm) than graphene but promise more *functionality*.

CNMs are mechanically⁴ and thermally⁵ stable (up to 1000 K) and can be chemically functionalised on one or even both sides⁶. The combination of this material being almost truly two-dimensional and suitable to be chemically tailored to a high degree makes it very interesting for: fundamental charge transport research, support grids for transmission electron microscopy⁷, nano electromechanical systems (NEMS)⁸, etc. Once full control is gained of CNM properties, functional devices based on molecules are within reach. For instance: annealing can bring a CNM to a highly ordered phase (locally), much like graphene⁹. By doing so, conductive properties can be tailored.

Self Assembled Monolayers (SAMs) are at the basis of CNMs. SAMs are spontaneously adsorbed and aligned, highly structured molecular monolayers *on substrates*. They are widely used for various studies in diverse fields (biophysics, surface physics, chemistry, etc.), both fundamental and applied¹⁰. Most of the SAM chemical properties are determined by the choice of molecules, which is why SAMs are very interesting to scientists. Chemists can design and produce functional molecules, thereby creating a *huge* amount of possibilities. It is even possible to make monolayers of mixed molecules for extra functionality¹¹. A nice feature regarding CNMs: chemical properties are partially passed on from SAM to CNM upon conversion (cross-linking of SAM-molecules)^{ii, 2}. This opens a route to *functional*, well-defined, freestanding two-dimensional surfaces. The research described here aimed to fabricate and characterise high resolution, laterally shaped CNMs. As a unique feature, we are using Low Energy Electron Microscopy (LEEM), which has many advantages over more conventional methods. This has led us to a new perspective on the process of *cross-linking*.

The process of making a CNM starts with the creation of a SAM. Choice of substrate, molecules and precise self-assembly method all depend on the desired properties to be given to the SAM. Many kinds of substrates can for instance be used: flat substrates like planar metals, silicon-oxide¹² and semiconductors¹³, and also curved ones like liquid mercury droplets¹⁴. A commonly used combination of substrate and molecules is a flat gold surface (e.g. Au(111)) and thiol terminated (HS-R) molecules, where HS is a thiol group and R represents the rest of the molecule. Together these can form a covalent Au-SR bond accompanied by release of H₂¹⁵. Two kinds of self assembly methods were used for this report, the solution method and the sublimation method.

After a SAM has been made, the SAM-molecules have to be interconnected in order to make a CNM. A process known as lateral *cross-linking* (or simply cross-linking). When molecular bonds are broken, the carbon radicals that are left can form new, intermolecular carbon-carbon bonds. This creates a network of interconnected SAM-molecules, which is a CNM. The initial cleavage of molecular bonds can be induced by irradiating a SAM with electrons¹⁷, UV photons¹⁸ or ions¹⁹. As it turns out, not all SAMs can be cross-linked. Alkane-thiol based monolayers have been shown to simply break upon electron irradiation²⁰. SAMs based on aromatic molecules on the other hand, have shown electron irradiation induced cross-linking¹⁷. See figure (1).

ⁱ This followed from the interpretation of the Mermin-Wagner Theorem.

ⁱⁱ The downside however, is that SAM defects are also passed on upon conversion of SAM into CNM.

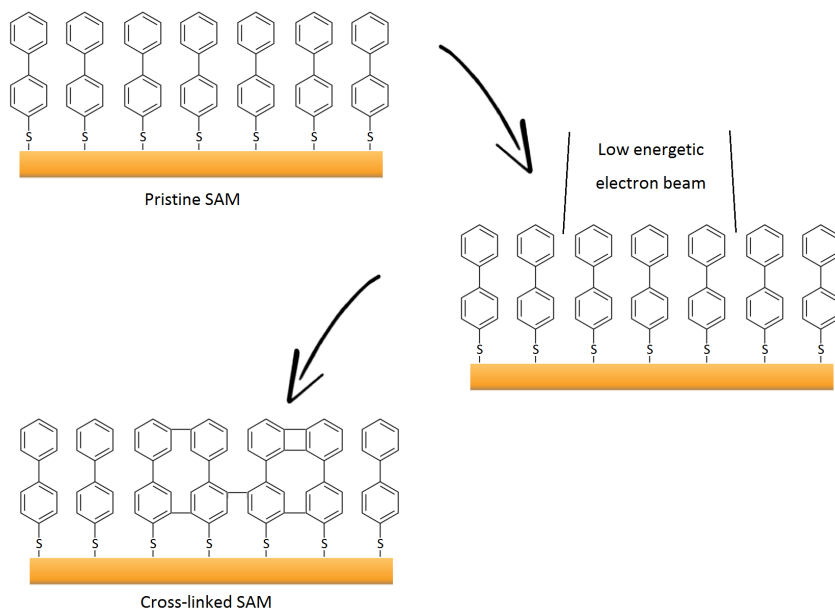


Figure 1: Sketch of cross-linking of pristine SAM (top-left) to locally cross-linked SAM (bottom-left) by local electron irradiation (mid-right). The SAM in this picture is made of biphenyl-thiol molecules, which is one example of an aromatic molecule.

The bottom-left picture of figure (1) shows a mixed molecular layer of (non) cross-linked SAM. In order to make a lateral patterned CNM, an extra development step is required. Cross-linked SAM can be developed by thermal annealing⁵. Which causes the non-cross-linked molecules to leave the substrate due to high thermal energy, while the substrate and cross-linked SAM are more stable at high temperatures. Alternatively, as was shown by W. Geyer¹⁷ *et al.* development can also be done by a wet-etching step.

The result is a CNM. However, it is still attached to the substrate. The final step: liftoff, is therefore optional, yet crucial for many experiments. Obviously, a sheet of nanometer thickness must be handled with great care. One clever solution is to make a locally freestanding CNM by transferring the CNM to a new substrate with holes²¹. For now, liftoff is beyond the scope of this research.

The goal of this report is to cross-link SAMs by electron irradiation. Using LEEM should allow us to irradiate very locally and give us excellent control over the electron energy and dose.

2. Methods

In short, we first want to make clean substrates which are then used to self assemble our molecules on. To see whether a well-defined layer was made we characterise our SAMs by conducting probe atomic force microscopy (CP-AFM) measurements. When the results are positive, we will irradiate these SAMs with the LEEM, which should induce cross-linking, thereby creating a CNM as was shown in figure (1) . We will now describe in detail the choices that were made and the methods that have been applied and how.

2.1 Sample preparation

Substrates

For this report, two kinds of substrates are used:

- Thermally evaporated poly-crystalline films of Au (30 nm) on Si (0.5 x 0.5 cm), with an adhesion layer of Cr (≈ 3.5 nm). Chromium and gold are evaporated at a base pressure $\leq 10^{-6}$ mbar with a typical rate of 0.2 respectively 0.8 \AA s^{-1} .
- Au(111) films (200 nm) on mica ordered from Phasisⁱⁱⁱ.

Cleaning

SAM defects can be introduced by a dirty substrate. Various methods were used to clean the substrate before SAM formation:

- UV/ozone treatment for typically 10 minutes, followed by thoroughly rinsing with ethanol.
- Rinsing with ethanol without UV/ozone treatment.
- Annealing by butane flame (≈ 800 °C)

Molecules

Our SAMs are made from 1,1'-biphenyl-4-thiol (BPT) molecules (see figure (2)). Which consists of two phenyl rings and a thiol group in series: $(\text{H}-(\text{C}_6\text{H}_4)_2-\text{SH})$. In general, the two phenyl rings will not be coplanar (unlike shown in figure (2)).

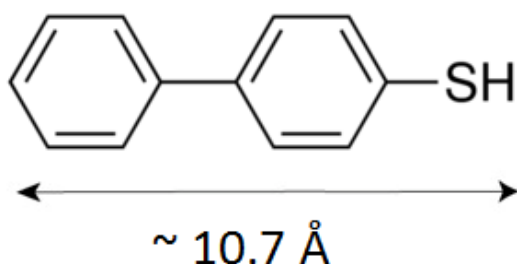


Figure 2: Molecular structure of a BPT molecule. It consists of two phenyl rings followed by a SH-group. BPT molecules are approximately 10.7 Å long.

Self assembly

SAM formation was done by the solution and sublimation method. Both are described:

- I. The solution method was applied by immersing one or multiple samples in a 10 mM solution of BPT in N,N-dimethylformamide (DMF) for roughly 72 hours. We give a simplified sketch of the process of self-assembly. First the thiol groups of the molecules will be chemisorbed, which makes them strongly bound to the Au substrate. This forms a molecular layer of flat-lying molecules. As time goes by, the surface density of adsorbed molecules increases and slowly, it becomes energetically more favourable for the molecules to go from the flat, unorganised

ⁱⁱⁱ www.phasis.ch

phase to a phase where they are all aligned and standing up straight. This phase change is driven by molecule-molecule interactions and can take several hours or even days¹⁶. The solution method is very sensitive to cleanliness of glassware, solvent and tools. The method was applied in both dry nitrogen atmosphere and in ambient conditions. After 72h, samples are taken out of the solution and cleaned by rinsing with DMF and ethanol.

- II. Samples are placed in a vacuum setup (figure (3)) where BPT powder is sublimated in the setup chamber by a combination of heat (60 °C water bath) and low (1 - 10 mbar) pressure. Meanwhile, the substrates remain at room temperature. The molecules self-assemble on the surface directly from the gas phase in roughly the same manner as in the solution method. A liquid nitrogen cold trap is used to avoid BPT molecules from getting into the rotary pump (Edwards FL20k Foreline trap). Sublimation was done in two stages: first active pumping followed by a waiting period without pumping (i.e. leaving the setup at vacuum). The total sublimation time and the ratio of active/no pumping have both been varied. In general, the total sublimation time is shorter than 72h, the absence of a fluid makes the molecule-molecule interactions more effective. In some cases, a cleaning step after sublimation of rinsing by DMF followed by ethanol was applied. The advantage is that this method is faster and can be combined with *in situ* observation techniques (e.g. microscopy and spectroscopy) due to the absence of a fluid.

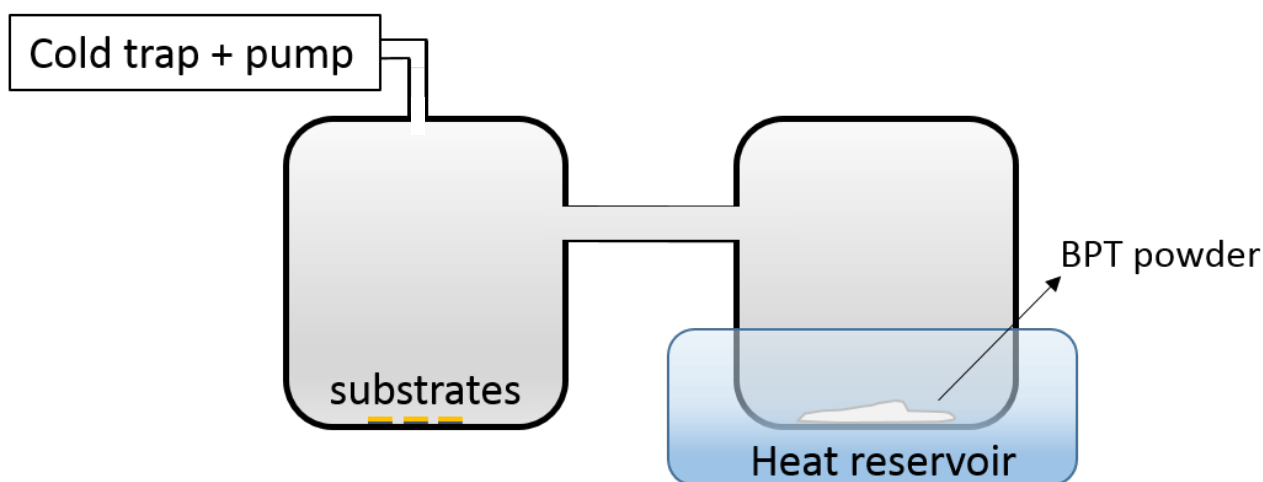


Figure 3: Sketch of our sublimation setup, it consists of two connected glass chambers, the left one is for the samples and the right one contains BPT powder on the bottom which is heated by a water bath (60 °C). Both chambers are pumped to vacuum (1 - 10 mbar) by a rotary pump. To prevent BPT molecules from getting into the pump, a liquid nitrogen cold trap is used.

2.2 SAM characterisation: Conducting probe atomic force microscopy

After the preparation of SAMs, they are characterised by conducting probe-atomic force microscopy (CP-AFM). This should provide information on the presence of a molecular layer on the substrate, resistance information and tell whether this layer is well defined or suffers holes. Before explaining CP-AFM, the working of (normal) contact-AFM will be explained (see figure (4)^{iv}).

In contact-AFM, a surface is probed by a very sharp tip (radius < 10 nm) which is at the end of a cantilever. A laser is reflected on the back of the cantilever to a photodiode. This photodiode is split into four quadrants. The location of the laser spot on the photodiode reflects tip position information. For example, a change in the tip height will result in a shift of the laser spot on the vertical axis of the photodiode. This way, height information can be retrieved while the tip is scanning the surface, this information is then reconstructed to a height map. The tip-surface distance is controlled by feedback on piezo crystals to avoid the tip from crashing into the surface.

^{iv} Source: http://www.ferroic.mat.ethz.ch/research/labs_general/afm/afm_img1?hires

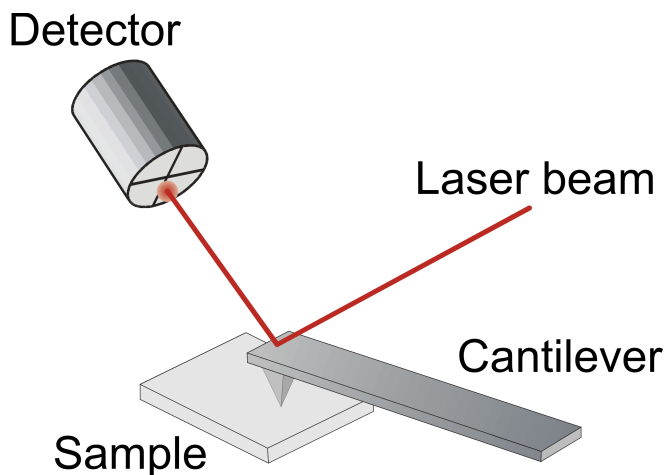


Figure 4: Sketch of the AFM basics, the tip at the end of a cantilever is 'feeling' the surface. The surface is scanned by slowly moving the sample while a laser spot reflected on the back of the cantilever brings tip position information to a four-quadrant photodiode.

The biggest differences between contact-AFM and CP-AFM are (i) that the latter uses a conducting tip (≈ 100 nm radius), Au coated in our case and (ii) that the surface is not scanned (due to rapidly wearing of the tip) but merely probed. The conducting tip combined with a SAM on a gold substrate gives a metal-molecule-metal junction (see figure (5)). Since the tip size is large compared to the area per molecule on a monolayer, not a single, but many molecules (100-500) are probed simultaneously. A force (referred to as the *load*) is applied to the tip on the layer and held constant by feedback controlled piezo crystals. If the load is too high, one would simply break through the SAM. On the other hand, if the load is too low, contact to the monolayer is lost, making the junction undefined and more subjective to noise. Less load also results in a higher resistance²².

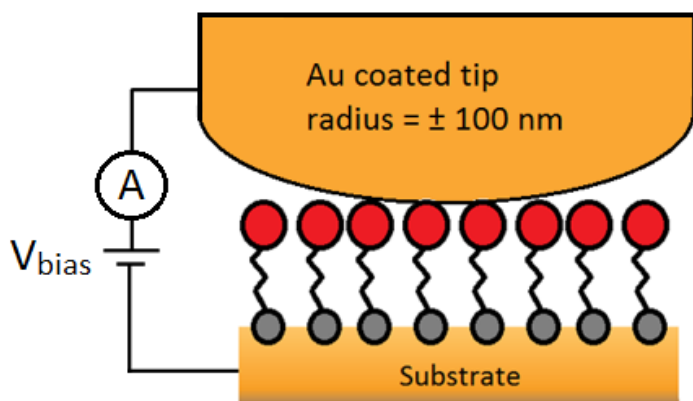


Figure 5: Sketch of a metal-molecule-metal junction in CP-AFM. Molecules are attached to a conducting surface on one end and probed by a conducting tip on the other. Therefore current will flow when a bias voltage is applied.

A ramp voltage (V_{bias}) is applied over this junction, sweeping from -1V to +1V and back. Meanwhile, electric current through the junction is measured at high rate and converted to a voltage by a 100 nA/V IV-converter (Bruker). Later, this voltage is calculated back to a current and plotted against applied bias voltage leading to an *IV-curve*. Typically 50-100 of these curves per spot are measured with one or two per second, which is repeated for 5-10 spots per sample. It is important not to measure too many curves on the same spot because the load can drift over time. This procedure was usually carried out for both 3.5 nN and 10.5 nN load.

After data acquisition, all the IV-curves retrieved from the same sample are plotted in one 2D-histogram (IV-histogram) where the ramp voltage is plotted against the measured current and the grey scale represents the amount of curves that overlap on that spot in the histogram. By numerical calculation, a dI/dV plot is obtained which is also represented by a 2D-histogram where the ramp voltage is plotted against logarithmically binned dI/dV . To make the dI/dV curve more smooth, slopes are averaged over a range of data points. We define the resistance of a molecular layer to be the reciprocal of the highest grey-scale value of the dI/dV -histogram at zero bias. Note that this value differs from the resistance through a single molecule since this method probes many molecules at the same time. It is assumed that this large number of molecules is similar for all our experiments such that resistance values as defined above can be compared. Both the IV- and dI/dV -histograms represent a full dataset without selection. Therefore, these histograms do not show any error bars as the error is implicitly incorporated via the spread in IV-curves.

It is instructive to show an example of CP-AFM data of a SAM we define as 'good', where the meaning of 'good' involves statistics and a low spread in data. Below, the 2D-histograms are presented of 726 IV-curves collected from 8 different spots on the same sample. Since the SAM is not exactly the same throughout the whole sample (e.g. due to local dirt or substrate step edges), there will always be some spread in IV-measurements. The data shown below however shows little spread indicating a well-defined molecular layer. At zero bias voltage, the variance in resistance is less than one order of magnitude which is considered to be small. The definition on SAM resistance also requires good statistics, which means enough IV-curves ($\approx 500 - 1000$) should be measured throughout the sample such that the data set is representative for the sample and statistically meaningful.

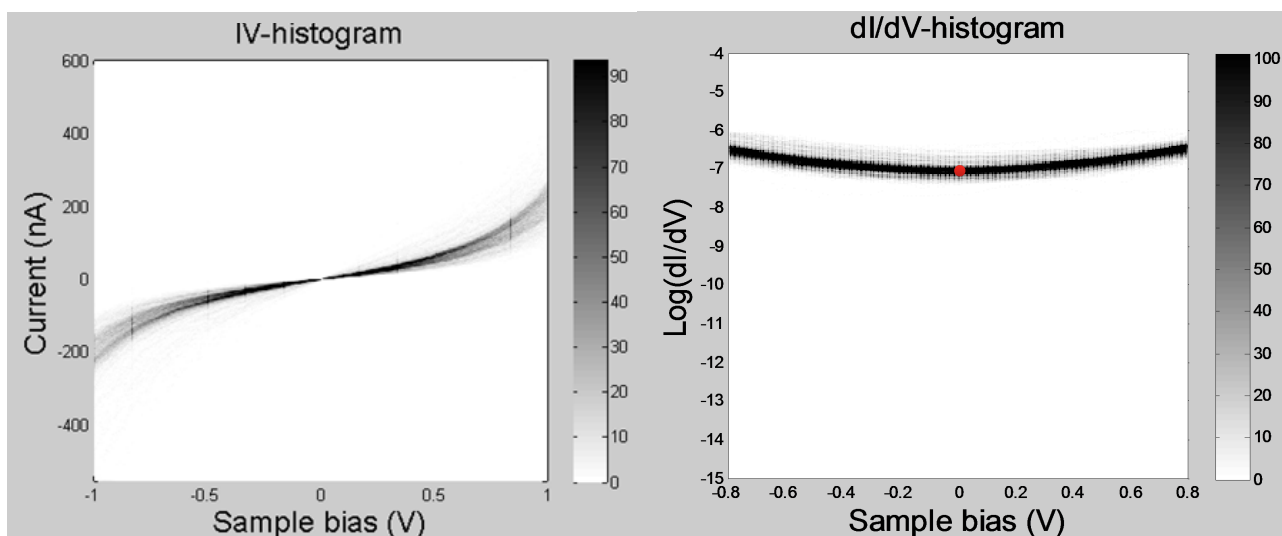


Figure 6: Example of CP-AFM results of a SAM marked 'good', meaning there is narrow spread in IV-curves combined with good statistics (i.e. large amount of IV-curves measured at various places on the sample). a) 726 IV-curves measured on the same sample are drawn in the same 2D-histogram, where the sample bias voltage is plotted against the measured current. b) dI/dV 2D-histogram obtained from a) by numerical calculation, here, the sample bias voltage is plotted against the conductivity. Using the definition mentioned before, a resistance of $\sim 6.3 \text{ M}\Omega$ (see red dot). This dataset was taken with a 3.5 nN load.

2.3 Low Energy Electron Microscopy

As was briefly noted in the introduction, a Low Energy Electron Microscope (LEEM) (part of the ESCHER setup at Leiden University) was used to achieve cross-linking of BPT SAMs. This is a unique feature of this research. Although cross-linking can be done with a normal electron gun as well, there are some clear advantages of using LEEM:

- LEEM and PEEM (Photoemission Electron Microscopy) can be used *during* irradiation by electrons and thermal annealing. This is done in real time, with video rate and a maximum spatial resolution of 1.4nm.
- LEEM allows for very local irradiation and excellent control of the beam, which is intended to be used for making laterally shaped CNMs in basically any shape which could lead to extra functionalisation.
- With LEEM, irradiating a spot with a size down to 5 μm diameter is possible. Combined with a high accuracy sample stage this allows for doing multiple experiments on the same sample.

In this section, the basic principles behind the LEEM will be explained briefly (see figure (7)). More detailed information can be found in reference 23. As the name suggests, a LEEM is an electron microscope and though small things are best imaged by small wavelength particles, low energetic electrons (thus 'long' wavelength by De Broglie) are very surface sensitive. As opposed to a normal (optical) microscope, LEEM uses an electron beam for illumination and instead of a set of optical lenses, in LEEM an image is formed by a set of electromagnetic lenses (i.e. electromagnetic fields that redirect electrons such that they work as a lens). From the electron gun, a focused beam of electrons is accelerated with an energy of 15 keV towards the sample. Just before reaching the sample surface the electrons are decelerated by an electric field to a well-defined energy in the range of 0-100 eV. This energy determines what will happen next. If the energy is negative or zero (the so-called mirror mode), electrons will not reach the surface. On the other hand, electrons with a positive landing energy will penetrate the surface a bit and interact with it (i.e. elastic scattering). In either case, at some depth, the same electric field that decelerated electrons towards the sample surface, now accelerates them away from it. However, this way, these electrons would go straight back to the electron gun. To avoid this, a magnetic field is placed between the gun and the sample, the Lorentz force will redirect the electrons coming back from the sample in another direction as those coming from the electron gun (think about the right-hand rule), thus the electrons of interest (carrying information about the surface) are directed towards the detector. The ESCHER setup is equipped with an extra electrostatic mirror to correct for spherical aberrations, making the resolution a factor 2 better compared to a commercial LEEM.

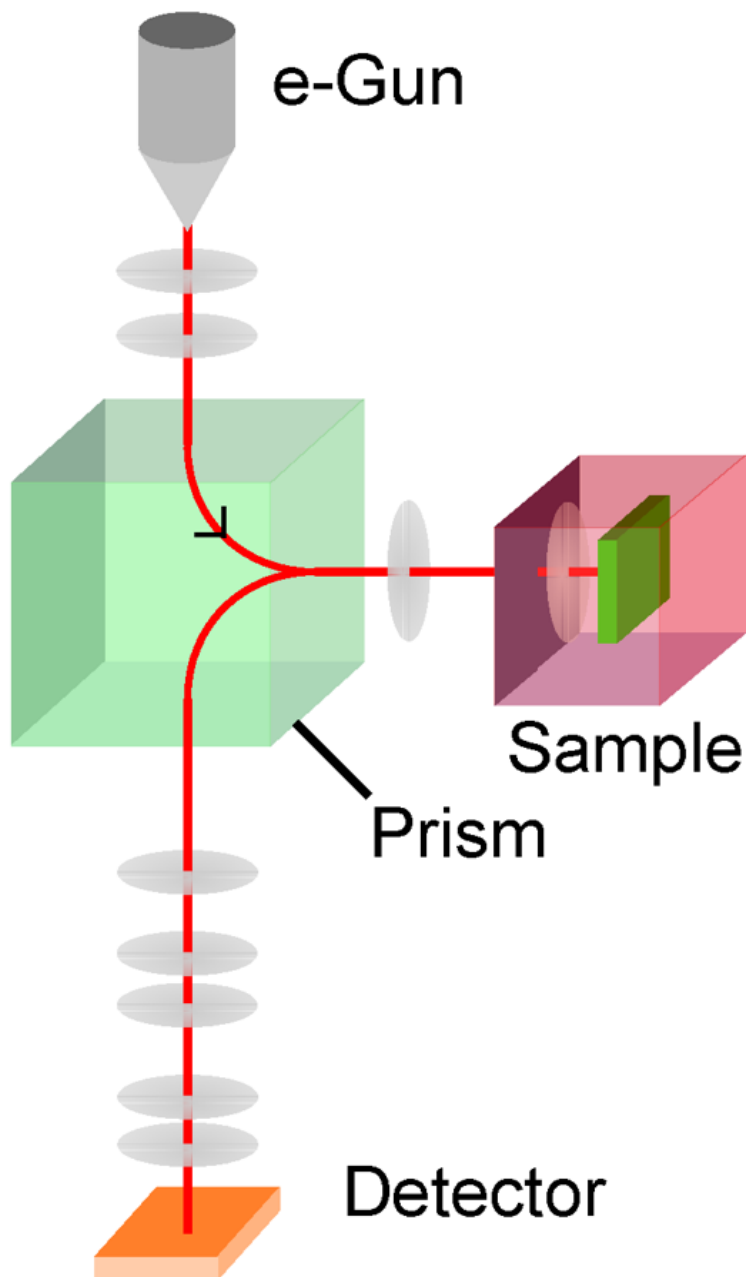


Figure 7: Sketch of the LEEM basics. A sample surface is imaged by electrons. These electrons come from the electron gun (e-Gun), are deflected by a magnetic prism (green block) and decelerated by an electric field (red block) to an energy of 0-100 eV. After interacting with the surface, electrons are guided to the detector. Figure made by J. Kautz and used here with permission.

Besides LEEM, the ESCHER setup can also do PEEM (Photoemission Electron Microscopy). In PEEM, the surface is illuminated by photons from a UV-light source (Hg discharge lamp) instead of electrons. Due to the photoelectric effect, electrons are emitted (which in turn may cause a cascade of more emitted electrons, so-called secondary electrons), these are then accelerated to the detector just like in LEEM. The energy of the emitted electrons is determined by the spatially varying photoelectric effect. The advantage of PEEM is that it has a bigger field of view ($\approx 150 \mu\text{m}$ diameter) than LEEM ($\approx 5 \mu\text{m}$ diameter), which makes it easier to find features and orient. The downside is the known fact that UV-light can also induce cross-linking of SAMs.

For cross-linking, two parameters appear to be of importance: the electron energy and the dose. The electron energy of our LEEM setup is limited to a range of 0-100 eV with a resolution of 0.1 eV. The dose, given by

$$D = \frac{I \cdot t}{A} \quad (1)$$

where A is the irradiated area (i.e. the LEEM spot size of ≈ 5 diameter), t is the time of irradiation and I is the electron gun current. The group of Turchanin *et al.*⁵ showed that electron induced cross-linking of BPT SAMs can be done by low-energy electrons and a dose of the order of mC/cm². Throughout our experiments the gun current was set on 2 μ A but slowly drifted upwards to ≈ 3 μ A. When all alignment is done properly, surfaces can be well imaged with ≈ 1 eV electrons. Since the alignment is energy-specific, increasing the energy puts the surface out of focus.

With LEEM, information on the surface's electronic structure can be obtained by a LEEM-IV measurement (not to be confused with the IV-measurements from CP-AFM). The LEEM signal intensity is recorded as a function of electron energy. This is done for every pixel in the field of view. In other words, a LEEM picture is taken on the same spot for each electron energy in a certain range. Note that this is an invasive measurement since the whole measurement is done on the same LEEM spot and energies can gradually go up to tens of eV. The result at a certain electron energy is affected by all the previous measurements on the same spot.

3. Results

3.1 SAM preparation

Appendix A shows an overview of all efforts in making SAMs for this report. Successful tries show up as green and failed tries as red. Where data is available, resistance as defined in the CP-AFM section is also reported. Note that the amount of BPT powder used for sublimation is not mentioned in the table. Yet, this amount was varied (typically 10 mg for 4h sublimation and 30 mg for 24h). However, for all sublimations it was observed that BPT was still present in powder form after 4 respectively 24 hours. Therefore, it should be sufficient to remark that *enough* BPT powder is used for all sublimations.

3.2 Testing UV light on BPT SAMs

The biggest field of view in the ESCHER setup is achieved by PEEM which exposes the surface to UV-light. To test the effect of UV-light on BPT SAMs, a sample with SAM is exposed to UV-light for two hours. The shape of a LEEM sample holder covers the edges of a sample, preventing those areas from being exposed. This is exploited to compare CP-AFM data of exposed and unexposed SAM from the same sample. Results are shown in figure (8).

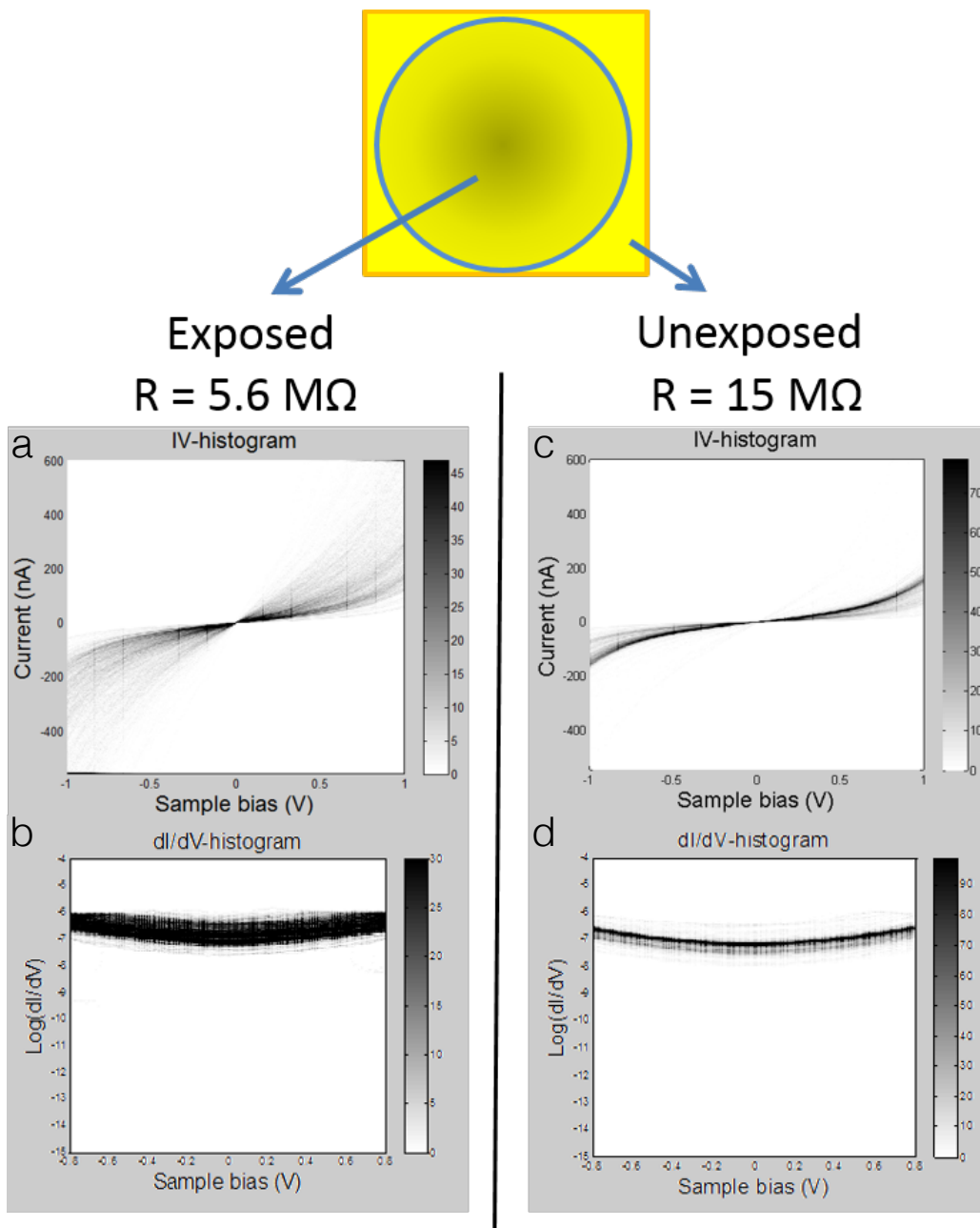


Figure 8: CP-AFM data of a SAM before (right) and after (left) two hours of exposure to UV light. a,b) IV-histogram and dI/dV-histogram of CP-AFM data of exposed area. c,d) IV-histogram and dI/dV-histogram of CP-AFM data of unexposed area.

The spread in resistance has clearly increased after this two hour UV exposure, which could be interpreted either as a decrease in SAM quality *or* as a partial cross-linking of BPT SAM. Either way, using PEEM should thus be avoided unless necessary. In future experiments, SAMs are exposed for no more than 30 minutes in total which is for now assumed to be a safe maximum.

According to literature, irradiation of BPT SAM with electrons induces cross-linking. This was tried for various combinations of dose and electron energy. Later on, we will take it a step further and develop irradiated BPT SAM by thermal annealing. However, first we will focus on an unexpected phenomenon that was observed.

3.3 Electron irradiation induced effect on BPT SAM

Some combinations of electron energy and dose systematically show irradiation-induced effects on the surface which are imaged in real time by LEEM. This effect starts right after irradiation and is imaged by LEEM with ≈ 1 eV electrons. An example is shown in the LEEM-video montage below:

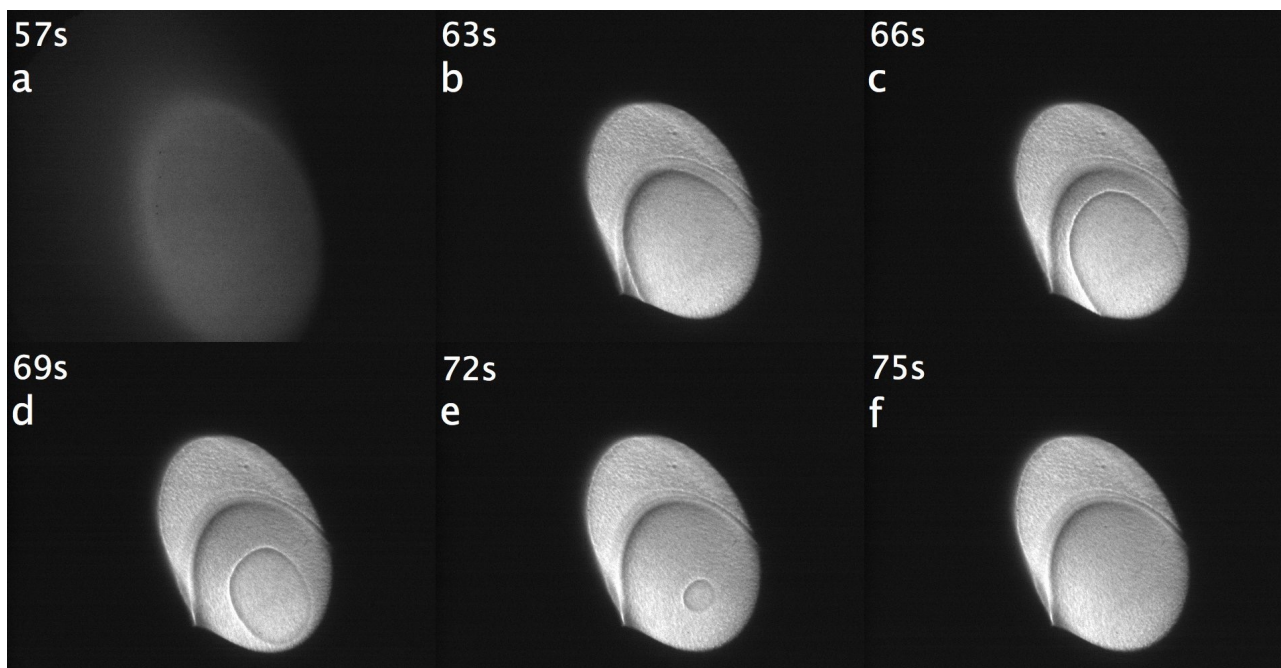


Figure 9: Montage of a single LEEM movie. The LEEM spot ($\approx 5 \mu\text{m}$ diameter) is used for irradiation of SAM for one minute by 40 eV electrons. $t = 0$ upon starting irradiation. a) LEEM picture during irradiation, since the alignment is energy specific, the surface is out of focus for higher electron energies (like 40 eV). All pictures from $t = 0$ to $t = 57$ s look the same and are therefore omitted. Pictures b) to f) show the LEEM image *after* irradiation. All show two ellipses, the outer one (where the LEEM spot *is*) and one that is only partially visible (where the LEEM spot *was* during irradiation). Imperfect alignment causes the spot to move a bit upon changing between high and low energy electrons. Furthermore, these pictures show a ring, starting at the edge in picture b), shrinking in c) to e) and finally disappearing in f)

Two results immediately stand out:

1. Irradiation has left an imprint on the surface, i.e. there is contrast between irradiated and non-irradiated areas.
2. A ring shows up at the edge of an irradiated area and shrinks until it disappears somewhere in the centre of the irradiated spot.

Imprints are basically always left on the surface after irradiation and are observed to lose contrast over time. By lacking knowledge of the collapsing ring's true origin, it will from now on be referred to as it is observed: a *front*. At this point, very little is known about this front. However, since it can be imaged with an *electron microscope*, the explanation that it is *some* kind of charge transport seems plausible. The front has also been observed to keep shrinking while the electron gun was turned off, this tells us it is *not* a LEEM artefact. Possibly, the front could be a signature of BPT SAM and indicate cross-linking (thus SAM to CNM conversion). It will be pursued to further investigate these suggestions in this report.

Figure (9) is also represented schematically in figure (10). This representation will later prove to be convenient when multiple illumination steps are used. The lower y-axis represents the radius of the front and is normalised by the size where it started, which is equal to the spot size. It is acknowledged that the front radius is not well defined since it is elliptically shaped. However, this plot has a purely qualitative function. After electron irradiation for a certain time, the electron energy is brought back to ≈ 1 eV. The time of irradiation and the electron energy during irradiation will hereafter be referred to as T_i and E_e respectively.

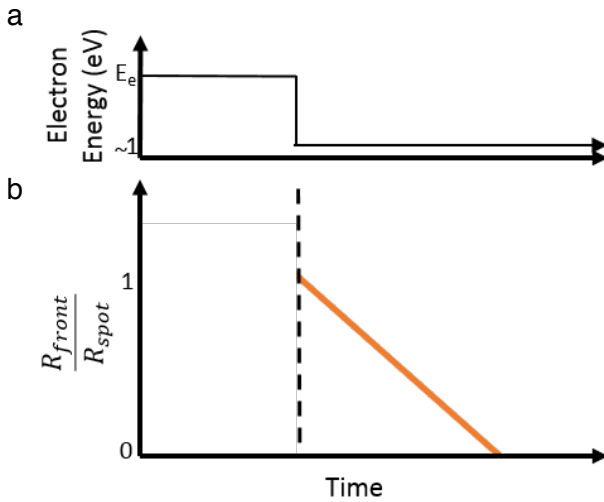


Figure 10: Schematic representation of a simple LEEM experiment. a) Electron energy of the LEEM beam as a function of time. b) Normalised front size as a function of time. After illumination with energy E_e , the front (orange line) appears and is seen in LEEM with ≈ 1 eV electrons. This front then shrinks over time.

Most experiments presented hereafter aim to discover the true nature behind this front. As was noted above, while some combinations of dose and electron energy do show a front, others did not. That brings up the question: why? By systematically going through a series of these combinations we attempt to answer this first question. Secondly, we aim to find out what process could drive the front movement, we do this by analysing the front's speed.

3.4 Structural investigation of the front

To find out what conditions on dose and electron energy are needed to create a front, E_e and T_i are systematically varied on a range of 5 to 65 eV and 5 to 70 s respectively. As dose scales linearly with illumination time (formula (1)), the x-axis in figure (11) may be read as dose up to some factor.

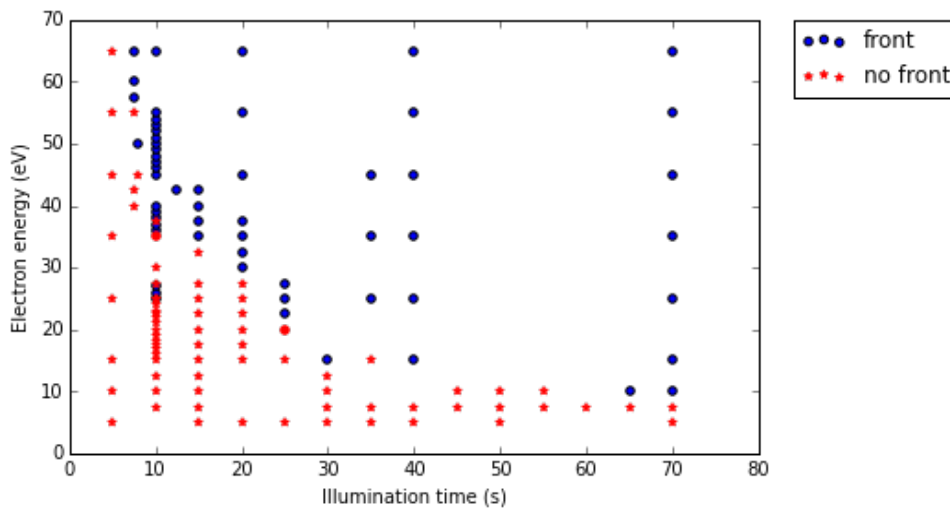


Figure 11: Plot showing whether a front is observed (blue dot) or not (red star) for multiple combinations of E_e and T_i . Data points were measured on three subsequent days during which the sample remained in the LEEM setup at ultrahigh vacuum. All data points represent a LEEM movie either showing a front or not which was judged by human eye.

The line dividing the blue dots from the red stars (hereafter referred to as \mathcal{L}) is a decreasing function. Furthermore, \mathcal{L} seems to follow a reciprocal relation. In the discussion, we will further investigate this suggestion by fitting the data to the function $E = a/t + b$.

Similar measurements but on a more limited range (5 to 45 eV and 5 to 40 s) have been conducted on another SAM on Au substrate which has qualitatively reproduced figure (11)^v. Furthermore, the front was also observed on a chromium substrate, presumably covered with sublimated BPT SAM.

3.5 Front quality/visibility

During the analysis of the data presented in the previous section, it became apparent that there might be a connection between the visibility of a front, and the (E_e, T_i) that induced it. The aim was to experimentally verify this by comparing pictures of different fronts made by the same T_i , but varying E_e . Thus moving 'up' in figure (11), away from \mathcal{L} .

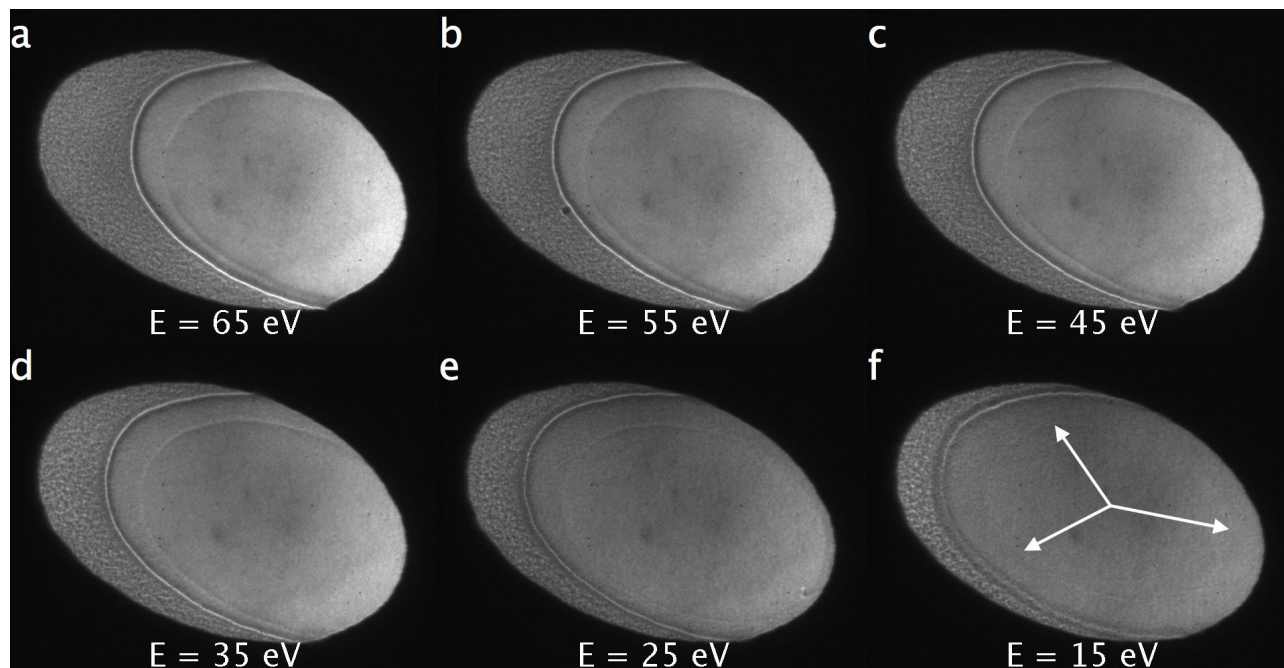


Figure 12: Series of LEEM-pictures of six fronts. All six spots were irradiated for 70 seconds but with different electron energies as indicated by the labels. After irradiation, a front was observed at all spots, these fronts were imaged by LEEM at a much lower energy of ≈ 1 eV. Here we compare their visibility. To make comparison easier, these pictures show the fronts at comparable size and position. For f), we have indicated where the front can be seen by white arrows.

Indeed, for $T_i = 70$ s there seems to be a relation between front visibility and E_e . The front is definitely less visible at 15 than it is at 65 eV. However, one could argue that the fronts in figure (a-d) are equally visible. 'Visibility' is not easy to quantify and therefore we refrain from doing so. Instead, the same data analysis as described above is performed for other values of T_i and also in the other direction (i.e. comparing visibilities at different T_i for constant E_e). This repeatedly shows qualitatively the same results.

Due to these results, it should be considered that some points marked as not showing a front in figure (11) actually do show a (very vague) front and vice versa^{vi}.

^v Qualitatively the same curve, but it appears to be shifted a bit, it is suggested that this shift is caused by the age of the sample as they slowly degrade in SAM quality (decreasing molecular surface density) over time.

^{vi} It also reveals a loophole that should be considered seriously. Possibly, all illuminations create a front but those fronts made by (E_e, T_i) below \mathcal{L} are simply too vague and overwhelmed by the noise in the LEEM signal.

3.6 'Frozen' front

The effect of a second irradiation on a pre-irradiated spot is now tested. To do this, there are two options: i) do irradiation *before* or ii) *after* the first front (*if* it was created) has disappeared.

Before continuing, the following notation is introduced: \mathcal{F}_n . Where \mathcal{F} indicates that we are talking about a front, and the subscript marks by which round of irradiation (first, second, ... , n-th) this front was induced. Both options mentioned above are now discussed:

i) Given that (T_i, E_e) are sufficient (according to figure (11)), it is observed that a new front (\mathcal{F}_2) is induced, which seems to behave the same in all aspects as fronts created on 'fresh' (i.e. not pre-irradiated) spots. Furthermore, when (T_i, E_e) are *insufficient*, second irradiation sometimes still yields a new front. Apparently, multiple irradiations stacked on the same spot can 'add up'.

ii) The observations of a second illumination on a pre-irradiated spot before the disappearance of the first front are schematically shown in figure (13).

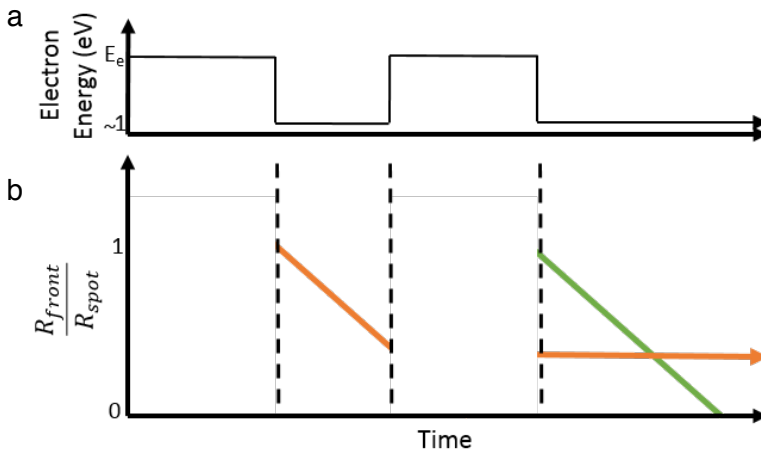


Figure 13: Schematic sketch of a LEEM experiment where a front (orange line) is made and frozen by a second illumination (second blue rectangle) on the same spot. This second illumination results in a new front (green line) and stops the first front from shrinking further.

From this drawing, one should note two things:

1. \mathcal{F}_1 (orange line) remains the same size after the second irradiation, it appears to be 'frozen'. Or in our notation $\mathcal{F}_1 \rightarrow \mathcal{F}_{1,f}$, emphasising that it is now frozen.
2. \mathcal{F}_2 (green line) is shrinking in size as usual and passes through $\mathcal{F}_{1,f}$.

We will now show that 'frozen' really means frozen, instead of moving very slowly. To do this, two size measurements are performed on $\mathcal{F}_{1,f}$ separated in time by a long period (compared to the typical timescale it takes for a front to disappear). The result is shown in figure (14). Note that the contrast does lower over time.

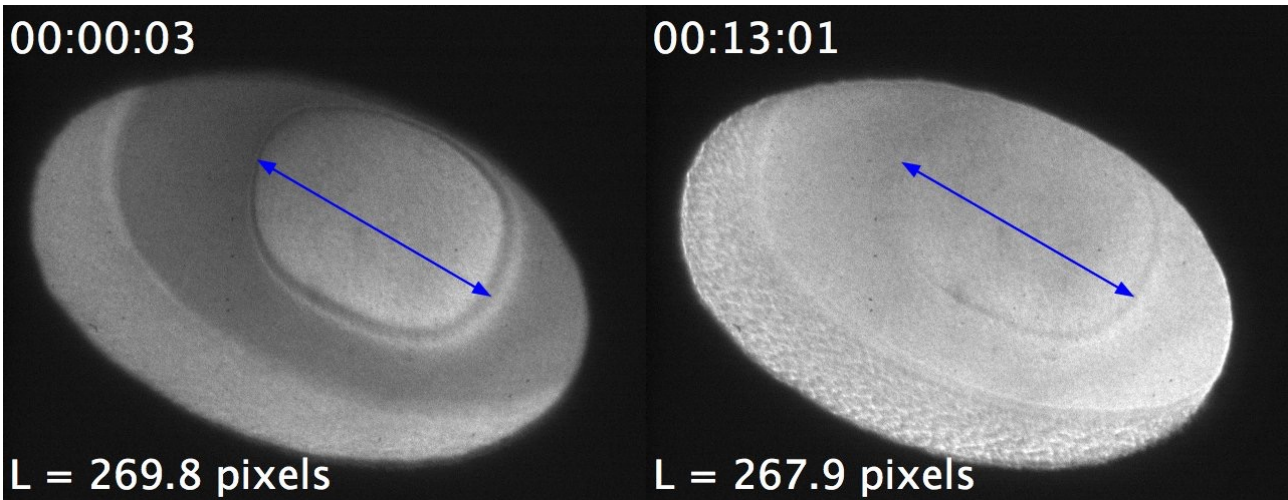


Figure 14: Two LEEM images of the same front. The front is created by 40 s illumination at 75 eV and was given some time to shrink. Then, the same spot was illuminated for 10 s at 75 eV causing the first front to stop shrinking. Time (labeled in upper-left corners) starts after the second illumination step, the last two digits are seconds. Lengths of the blue arrows are in the lower-left corners (measured in pixels). The error in this length measurement is estimated to be ± 3 pixels.

As noted above, \mathcal{F}_2 is observed to move through $\mathcal{F}_{i,f}$ without any *visible* interaction. However, we will later show that data indicates something has to change at areas where $\mathcal{F}_{i,f}$ is passed by \mathcal{F}_2 .

We now move on to *three* subsequent irradiations on the same spot (assuming the second irradiation was sufficient to create \mathcal{F}_2). Again, there are two options, irradiate either *before* or *after* $\mathcal{F}_{i,f}$ is passed by \mathcal{F}_2 . Both options and observed outcomes are schematically shown in figures (15) and (16).

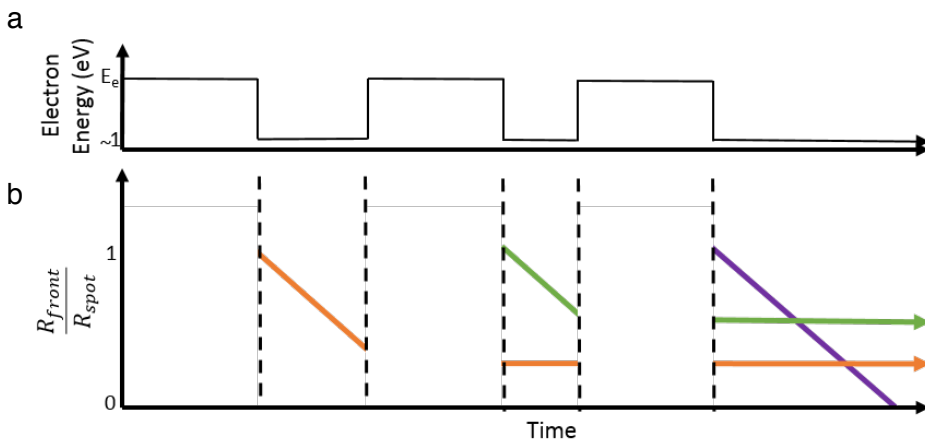


Figure 15: Sketch of three illuminations and observations, the third illumination is applied before the second front passed the first (frozen) one. This results in a new front (purple line) and freezing of the second front.

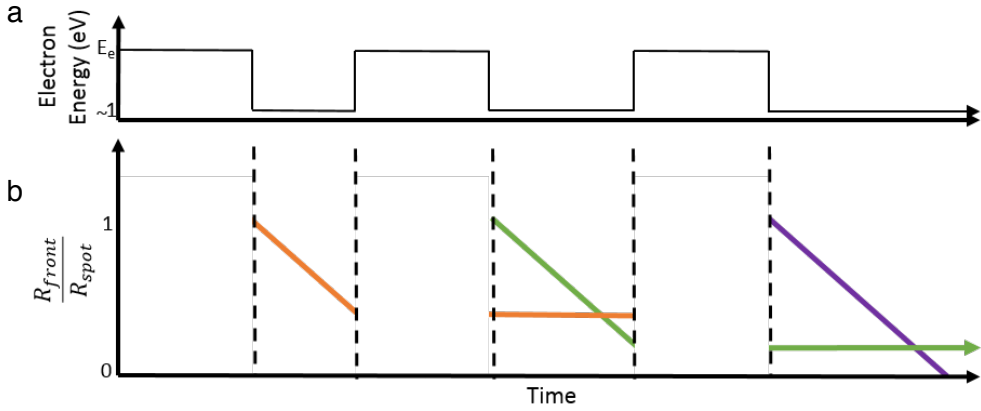


Figure 16: Sketch of three illuminations and observations, the third illumination is applied after the second front passed the first (frozen) one. A new front (purple line) is created while the second (green line) becomes frozen and the first vanishes.

Knowing the outcome of the previous experiments, the first case is quite predictable (though not trivial): $\mathcal{F}_{1,f}$ remains frozen, \mathcal{F}_2 is frozen and \mathcal{F}_3 is created. The second case will now be studied in more detail. Experimental data is shown in figure (17). As can be seen, $\mathcal{F}_{1,f}$ is present before, but gone right after the third irradiation, which was done between picture ii) and iii).

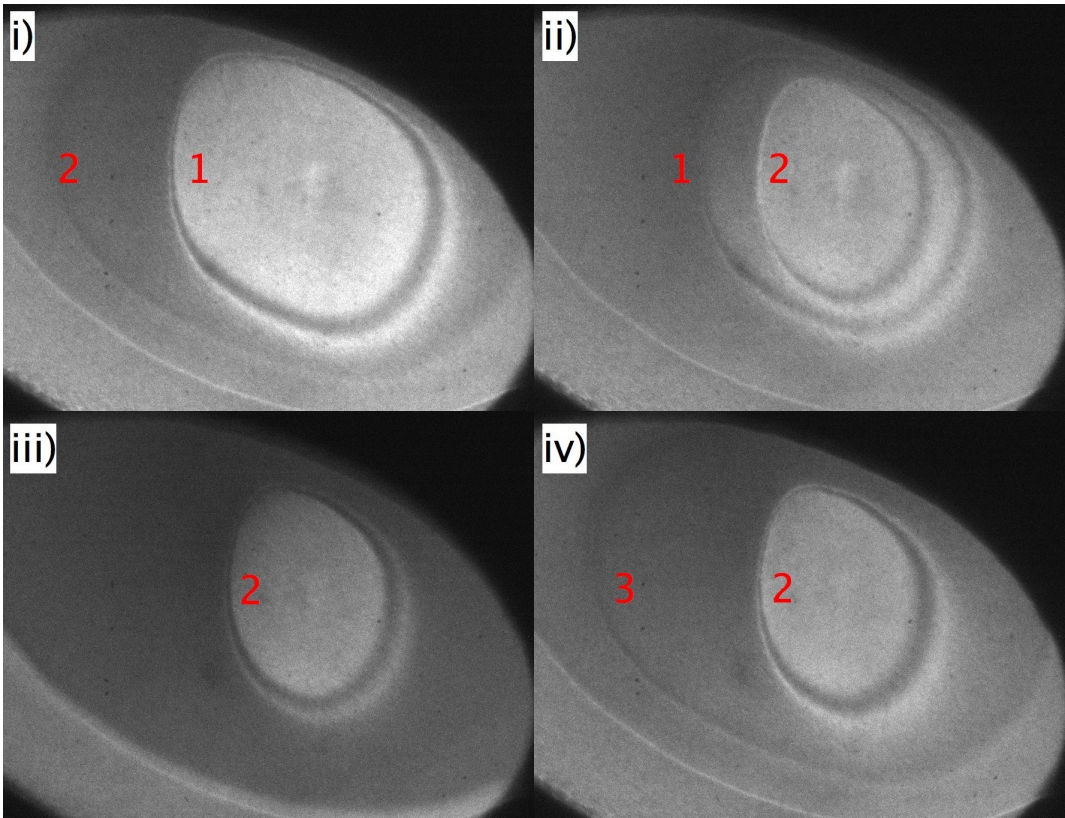


Figure 17: LEEM movie montage. The same spot is irradiated three times for respectively 15, 40 and 20 seconds at 75 eV. The third irradiation is done between picture ii) and iii). Red numbers indicate the front number (first made, second made etc.). Thus the first two irradiation steps were done prior to picture i).

3.7 Detailed analysis of front speed

The straight, coloured lines in figures (10), (13), (15) and (16) suggest a front shrinks with constant speed, here we question whether this is true. To answer this, a LEEM-video with a front is analysed

in detail. To measure the front's position over time, we have used intensity profiles along a line starting at the front centre and ending at the edge (see figure 18a). To reduce noise, intensity was averaged over a width of w pixels. One example of such an intensity profile is shown in figure (18b), similar profiles are made for all video frames between the front starting and disappearing.

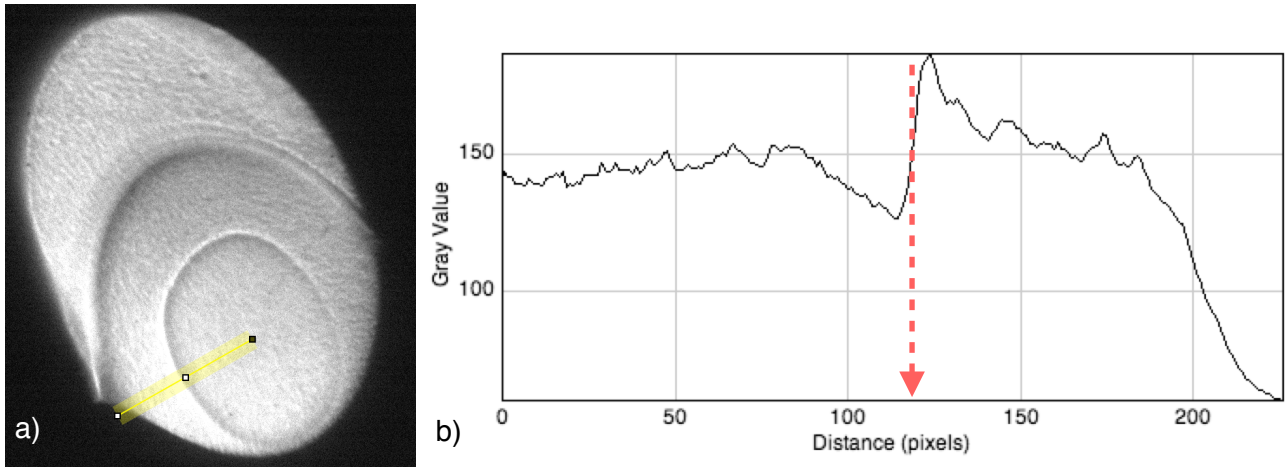


Figure 18: a) Picture of a LEEM spot, an intensity profile is calculated along the yellow line. To reduce noise, intensity is averaged over the width of this line (30 pixels in this picture). b) Intensity profile calculated along the line illustrated in a). We have defined the position of the front to be the distance from the centre to the pixel in-between low and high intensity, where the slope is maximal, as indicated by the red arrow. The point of maximal slope is estimated to be determined within ± 1 pixel.

Front position was defined as the transition point from low to high intensity, where the slope is maximal. Front position data is shown in figure (19a).

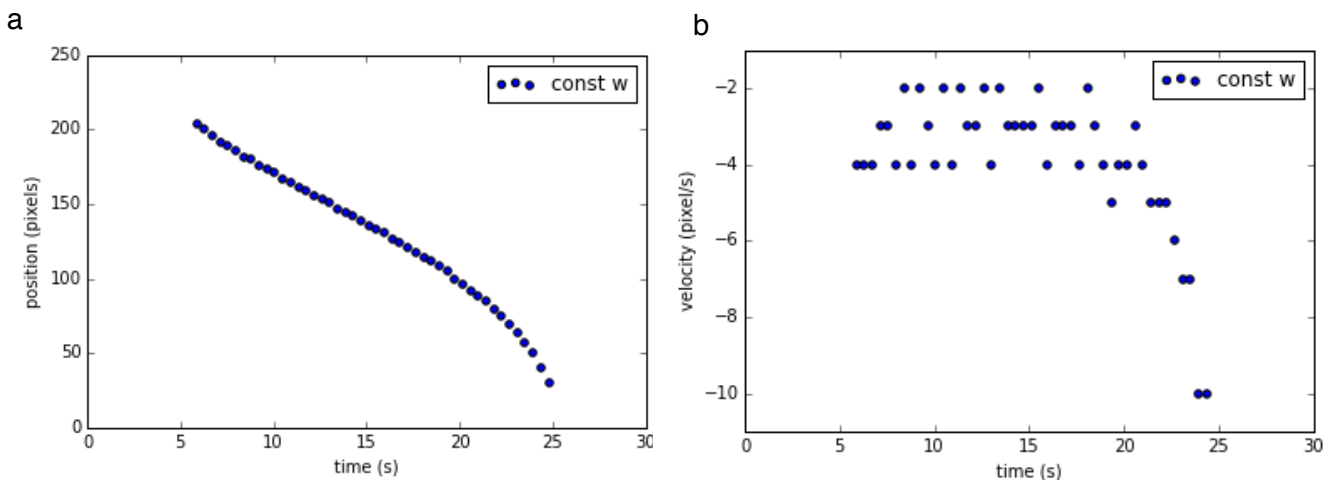


Figure 19: Front speed data measured with a constant w (30 pixels). a) front position. b) Front velocity data extracted from position data by calculation of the slope between two subsequent points. Note that this method is sensitive to bit-noise. Frame number is converted into time by knowing that the time between two frames is ≈ 0.42 s. Position of zero pixels is the point where the front disappears.

Next, the slope between every two subsequent points is calculated and plotted as a function of time (figure (19b)). These plots suggest an acceleration of the front just before its disappearance.

As is shown in appendix B, the method used to obtain the result above is not perfect and introduces an artificial acceleration towards the end. However, comparison of between results measured by the 'wrong' method a more proper method show that this artificial acceleration is very small. Both methods were used to determine the front position, the difference between these two measurements is minimal, 1 pixel difference on a ~ 40 pixel radius front. Therefore, it is concluded that figure (19) is correct and that the acceleration is real.

Now that the speed of a single front has been investigated, we would like to know whether front speed depends on E_e and T_i . However, front speed was shown not to be constant, which calls for a

clear definition of front speed for comparison of multiple fronts. Figure (19a) shows the front position to decrease linearly in time for roughly the first half of its lifetime covering a bit less than half of short axis LEEM spot radius. We define the slope on this linear part to be the speed of a front. Using the above definition we measure front speeds by simple two-point measurements, results are shown in figure (20).

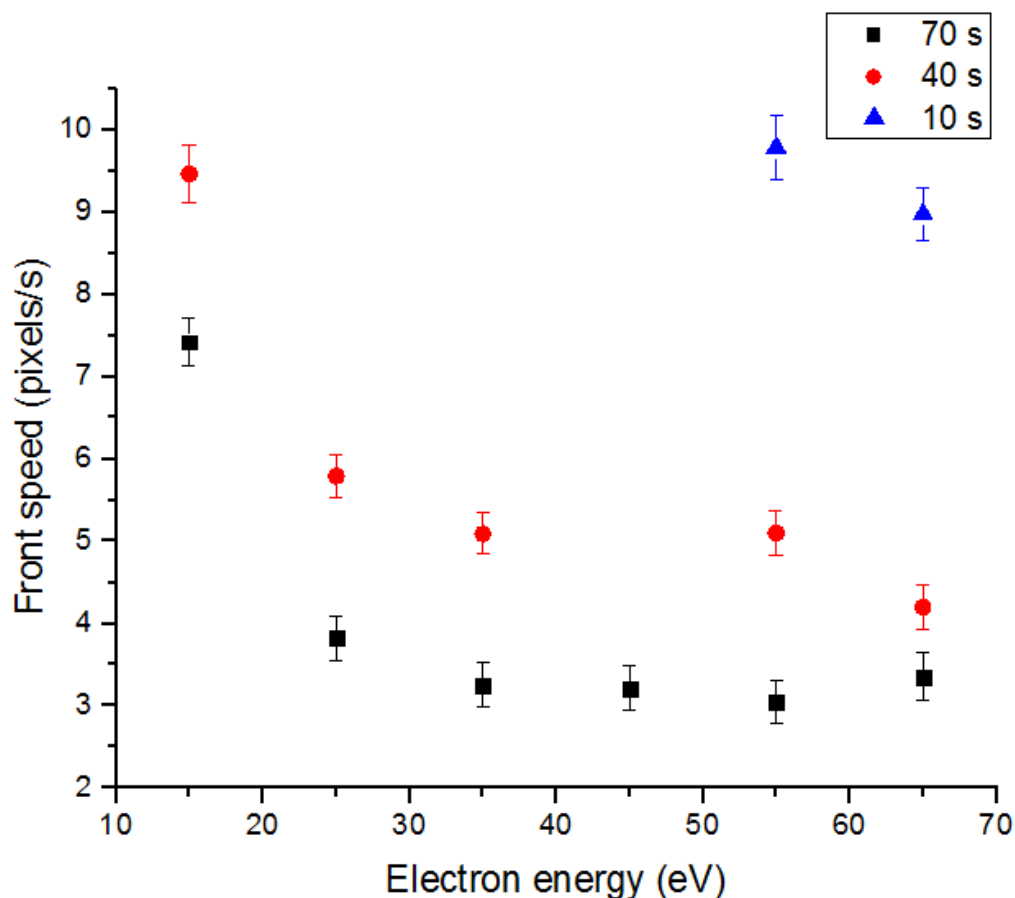


Figure 20: Measured speeds of fronts created by different (E_e , T_i). Colour (black/red/blue) indicates T_i . The horizontal axis shows E_e and front speed is shown on the vertical axis.

3.8 Developing illuminated SAMs

It is attempted to cross-link BPT SAM and to find out whether there is a correlation between the front and this cross-linking. A pattern of high and low E_e illuminated spots is made on a straight line on SAM:



Figure 21: Sketch of a pattern of illuminate spots made on SAM (grey background). Red and blue spots mark $E_e = 75$ eV and $E_e = 20$ eV respectively, for all spots: $T_i = 20$ s. Spot size (long axis) is approximately $5 \mu\text{m}$, length between two spots (centre to centre) was set on $10 \mu\text{m}$.

Hereafter these spots will be referred to as R and B (as in Red and Blue as indicated in figure (21)). R is irradiated at 75 eV, B at 20 eV and all spots are irradiated for 20 seconds. In accordance with previous results, R shows a front after irradiation, whereas at B, no front is observed. By thermal annealing, SAM-molecules that have not been cross-linked should desorb from the surface. Cross linked SAM however is more firm and acts as a negative resist for annealing. Thus: *if* the front is a sign of cross-linking then *only* R is expected to give contrast with the substrate *after* annealing.

After thermal annealing at ± 180 °C for six hours two important observations are made:

1. Both R and B are seen in both LEEM and PEEM (figure (22a)). As can be seen, R shows higher contrast.
2. Imprints are still left on the surface upon irradiation by 75 eV for 20 s, but the front is no longer observed.

The exact same observations were made after five more hours of annealing at 300 °C (figure (22b)). Which implies that the surface is not bare gold (but is still covered by some dirt or a low surface density SAM). Therefore, one last heating for 16 hours at 540 °C (figure (22c/d)) was done. Whereas nothing changed regarding the second observation, B now appears to be indistinguishable from the gold surface. Meanwhile, R still show contrast.

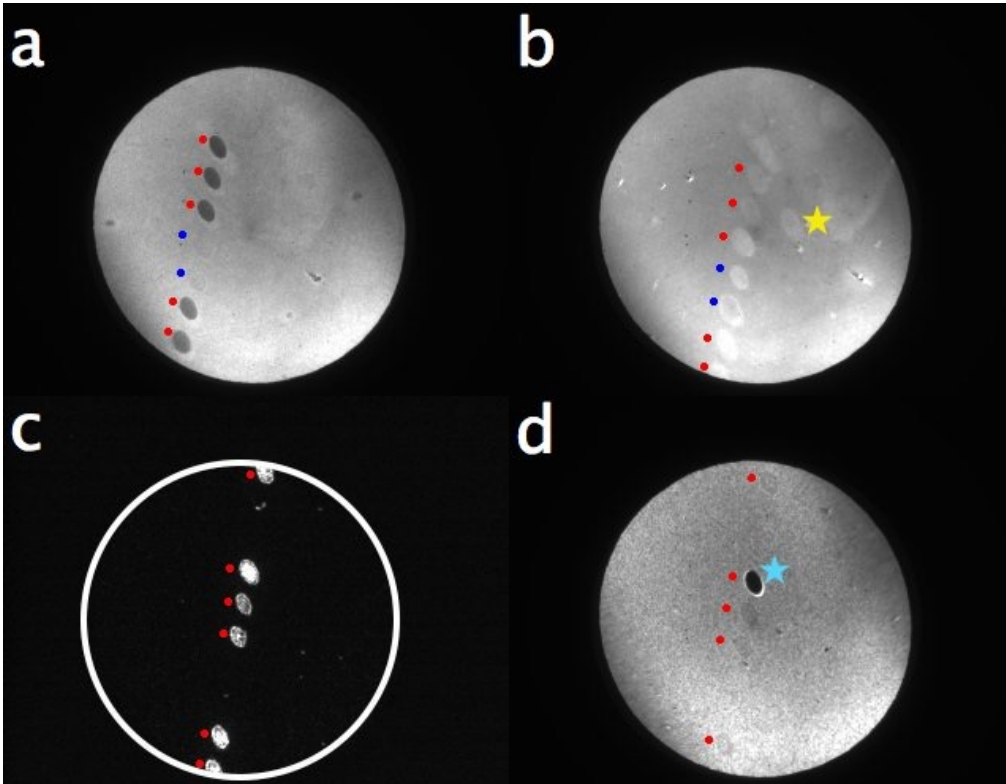


Figure 22: PEEM pictures of the illuminated pattern. Picture made after a) 180 °C annealing for six hours, b) five more hours annealing at 300 °C, c) another 16 hours annealing at 540 °C while sample is ≈ 130 °C, d) after cooling down. Red/blue points indicate R/B spots according to the pattern. The yellow star indicates a spot that was illuminated after annealing, which left an imprint. Blue star marks a spot where a LEEM-IV measurement was conducted just prior to making this picture.

LEEM-IV's are measured at R after the final annealing step, the results are shown in figure (23). These measurements show that a structure is left, which appears non-uniform and suffers various holes. Furthermore, the same measurement on B shows that these spots have become indistinguishable from the substrate after all annealing steps.

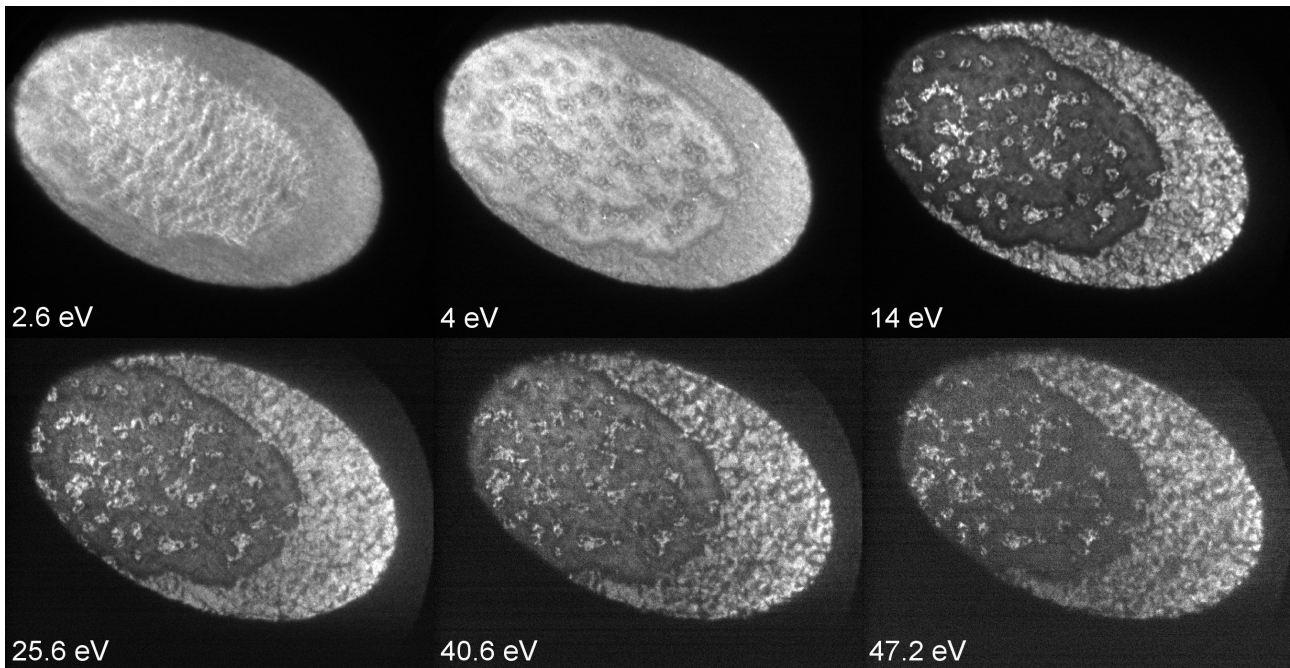


Figure 23: Montage of a LEEM-IV measurement on R. LEEM-IV was made in bright-field to keep good contrast up to high energies. Labels correspond to electron energy. The structure (dark area in pictures 4 - 6) clearly shows some holes. These holes look the same as substrate outside the structure.

The LEEM-IV measurement is used to make LEEM-IV curves. To smoothen the curve, intensity is averaged over a circle (≈ 20 pixels radius). Three LEEM-IV curves (figure (24)) are made: i) on the structure (yellow dot), ii) on substrate outside this structure (blue dot), iii) on a hole inside the structure (green dot). Results are shown in figure (25).

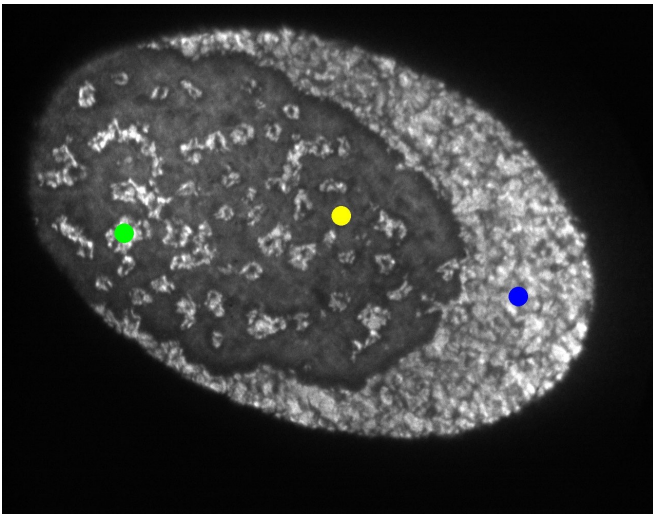


Figure 24: One frame of a LEEM-IV measurement, we have indicated by a yellow (on the structure), blue (gold substrate outside structure) and green (on a hole in the structure) dot where LEEM-IV curves are made.

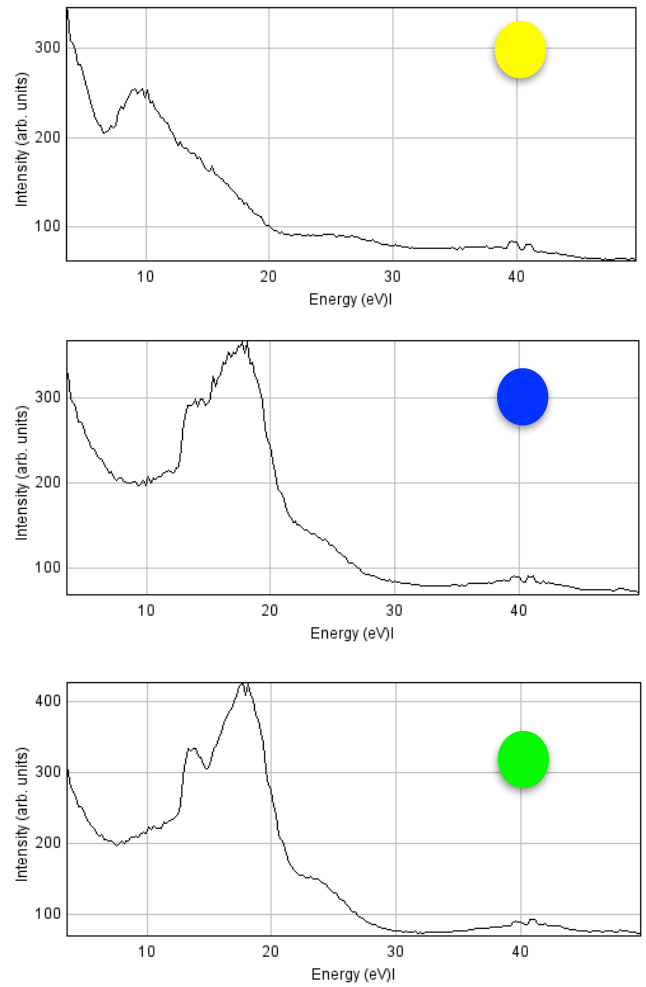


Figure 25: Three LEEM-IV curves taken on the structure (top), gold substrate outside the structure (middle) and on a hole in the structure (bottom).

The curve on the new structure shows a dip at ≈ 7 eV and a peak at ≈ 9.6 eV. Note that the LEEM-IV curves on the substrate and on a hole on the structure are very similar, both show a dip at ≈ 9.3 eV, and a peak at ≈ 17.6 eV with a shoulder at ≈ 14.1 eV telling us this new structure indeed suffers holes.

4. Discussion

4.1 SAM results

A critical look at table (1) (see Appendix A) reveals that the solution method did not deliver many good results. This is mostly due to the large spread in resistance which is frequently (though not always) measured with CP-AFM on solution made SAMs. The amount of spread in resistance can be inferred from the dI/dV histogram band thickness at zero bias voltage. For the solution method, this spread is observed to be up to 4 orders of magnitude, while the for sublimation method, this is mostly 1 - 1.5 orders. However, the average resistance values are mostly similar for the solution- and sublimation method made SAMs. This gives us more confidence that our SAMs are truly monolayers instead of multilayers.

We will now compare our resistance values of BPT SAMs on Au(111) ($\approx 9 \text{ M}\Omega$) with those found by other groups.

First, we compare with the group of Kim BongSoo *et al.*²⁴. They have reported a measured resistance $\approx 1 \text{ M}\Omega$ for naphthalene-2-thiol (NaphSH) solution-made SAM. Their measurement was also done by a conducting tip and SAM substrate (both Au). Just like BPT, NaphSH is a conjugated molecule. However, there are also a few differences: (i) ≈ 100 molecules were estimated to be probed, (ii) a load of 1 nN was used, (iii) NaphSH is a slightly shorter molecule (about 1.5 Å). We conclude this resistance value to be a bit off with ours. This seems plausible, we have estimated to probe more molecules and have used a bigger load but since BPT is a slightly longer molecule, this results in a higher resistance.

Furthermore, the group of Takao Ishida *et al.*²⁵ reports a resistance of 1 - 1.1 M Ω for 4-biphenylmethanethiol solution made SAMs. Measured by similar conditions (1 nN load, 100 nm tip radius).

Finally, we compare with the group of Paul Penner *et al.*²⁶, where a value of $575 \pm 4 \text{ }\Omega \text{ cm}^2$ was found for the resistance of BPT SAM. However, their measurements were conducted by a different method. The biggest difference is that a eutectic Ga-In layer as a top electrode was used instead of a Au coated AFM tip. They have estimated that 69 junctions were measured but present resistance information in a scale-independent form. To make this value comparable, we divide their value by the estimated tip/SAM contact area of our measurements. We estimate this area to be a circle of 20 nm radius. This calculation leads to a resistance value of $\approx 10^{14} \text{ }\Omega$. Which is about seven orders of magnitude higher than our measurements and the previously compared groups.

These comparisons show that our measured resistance is probably in the right order of magnitude. However, it must be noted that although NaphSH and biphenylmethanethiol are of comparable length with BPT, they are different molecules. Further research is needed to confirm that our BPT SAMs are truly of monomolecular thickness and not stacked multilayers.

UV-light exposure of BPT SAM

It was shown that UV exposure of BPT SAMs increases the spread in resistance measured by CP-AFM. This can be explained in two ways: (i) SAM has decreased in quality (i.e. a lower molecular surface density) due to exposure to UV-light. (ii) SAM has (partially) been cross-linked by UV-light exposure which also leads to a higher layer resistance²⁶. Based on the present data, neither of the two explanations can be ruled out. In the outlook, a possible future experiment will be proposed. SAMs used for other experiments have never been exposed to UV for more than half an hour. However, it is unknown whether the process driving the increasing spread in resistance is linear in time or not. In a non-linear case, it is very well possible that most damage is done in the first few minutes of exposure. More investigation would be needed to arrive at a conclusion.

It is verified that a front can still be induced after exposing SAM for 15 minutes to UV. However, this does not lead to any conclusion while it is unknown what this front exactly is. Mixing these two methods (i.e. expose for a certain time and then check for front and then collect CP-AFM data) could be useful.

4.2 Front interpretation & energy-dose

We now ask ourselves what the front might be and where it could originate from. We give a few suggestions: i) charging of the SAM surface, ii) reorganisation of molecules, iii) shifting of molecular levels, iv) a ring of charge. Based on our measurements, suggestion iv) can be ruled out, which will be explained. In section 3.7, it was shown that a front shrinks linearly in time during roughly the first two-third part of its lifetime and to slightly accelerate after that. This implies that the front should *not* be interpreted as a ring of charge (neither positive nor negative), for if this were the case, electrostatic repulsion of like charges would increase during the shrinking of the ring, which would cause a deceleration towards the end.

Next, we discuss figure (11), which shows that some combinations of (E_e , T_i) do induce a front, while others do not. Clearly, the distribution of blue dots and red stars tells us that the appearance of a front is not determined randomly. Figure (11) hints that a decrease in either E_e or T_i , can be 'compensated' for by an increase in the other variable. In other words, fronts can be created at very short T_i but this requires high E_e . Or, the other way around, for fronts created by long T_i , a low E_e is sufficient. We will now discuss the physical meaning of the apparent reciprocal relation between electron energy and illumination time. It is emphasised that this part of the discussion is a bit more speculative.

Points that should represent \mathcal{L} are extracted from the data in figure (11) by taking the average of the highest red star and the lowest blue dot for all t where possible. These points are fitted to the function $E = a/t + b$, the result is shown in figure (26).

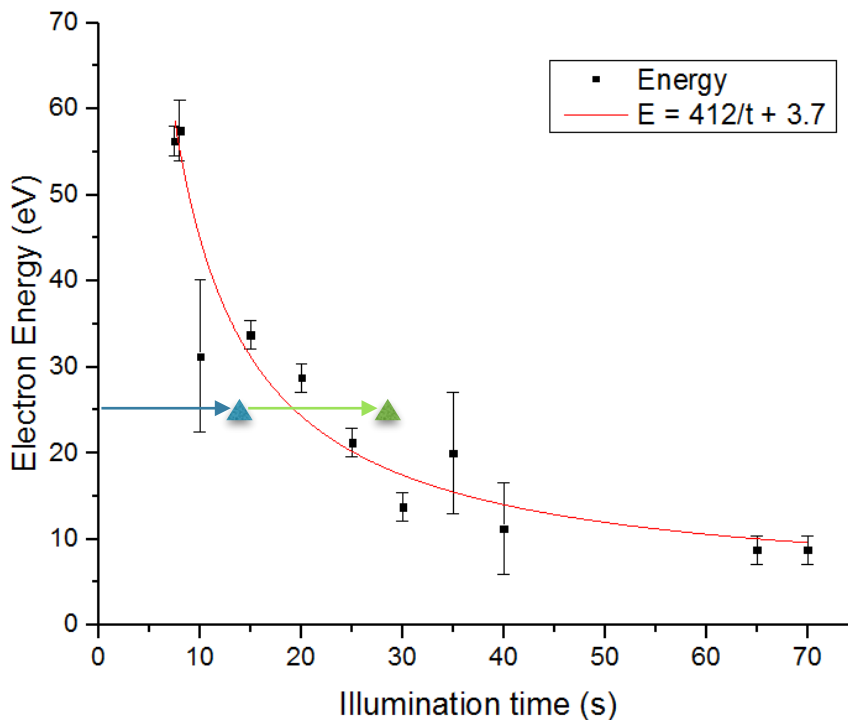


Figure 26: \mathcal{L} fitted to the function $E = a/t + b$ (red line). Fit values for a and b are found in the legend with relative fit errors of $\approx 6\%$ and $\approx 52\%$ respectively. The error bars scale with the distance between the highest red star and lowest blue dot. The arrows (making irradiation steps) and triangles illustrate how two subsequent irradiations can yield a front, whereas individually they would not.

If a reciprocal relation between illumination time and electron energy exists, there is in essence only *one* meaningful variable, which is the combination of electron energy and irradiation time. We will refer to this variable as energy-dose (Π). In formulas:

$$E \propto \frac{1}{t} \rightarrow E \cdot t \propto C \rightarrow \Pi \equiv E \cdot D = \frac{I}{A} = C'$$

Where C and C' are some constants and we have used formula (1) in the last step. This formula implies that Π is constant along \mathcal{L} . The fit of \mathcal{L} to the function $E = a/t + b$ reveals a slight complication, according to this fit, the value of b is non-zero. The formula is rewritten to find the physical meaning of b :

$$E = \frac{a}{t} + b \rightarrow t(E - b) = t \cdot E_{\text{eff}} = a \rightarrow \Pi_{\text{eff}} = D \cdot E_{\text{eff}} = \frac{I \cdot a}{A} = \text{const}$$

Note that b must have the unit of energy and acts as an offset. Therefore, we interpret it to be a threshold energy. We will from now on refer to this threshold energy as E_t instead of b . In the outlook, an experiment set to determine E_t will be illustrated.

Next, we now suggest that E_t is equal to the energy needed to break a single carbon-hydrogen bond within a BPT molecule. This implies that a primary electron with energy $3E_t$ can break at most three bonds. A formula will be derived for the number of possibly broken bonds per BPT molecule (N_{mol}). This formula should scale linearly with the number of bonds *one* primary electron can break: E/E_t . This should be multiplied by the total amount of primary electrons shot at an area of one BPT molecule (A_{mol}):

$$\frac{I \cdot t}{e} \cdot \frac{A_{\text{mol}}}{A}$$

If we plug all this in a formula for N_{mol} we get:

$$N_{\text{mol}} = \frac{E}{E_t} \cdot \frac{I \cdot t}{e} \cdot \frac{A_{\text{mol}}}{A}$$

Up to now it was implicitly assumed that *if* a CH-bond can be broken, it will *always* happen. However, it would be more plausible if some kind of chance is involved: β . Furthermore, we imagine this β in general to be a function of energy. After plugging in β we have:

$$N_{\text{mol}} = \frac{E}{E_t} \cdot \frac{I \cdot t}{e} \cdot \frac{A_{\text{mol}}}{A} \cdot \beta(E)$$

Data suggests some kind of ‘addition rule’ for stacked irradiations, or, in view of what is discussed above, the addition of energy-doses. This implies that the history of local irradiations is memorised for a certain period. We have illustrated in Figure (26) how this could work. Consider the situation of two consecutive electron irradiation steps on the same spot. The first being insufficient to create a front and the second being the same, but applied right after the first. The first irradiation, (indicated by a blue arrow) brings us to a point below \mathcal{L} (blue triangle). But, the second irradiation (green arrow, same length and direction) ends *above* \mathcal{L} (green triangle) meaning a front is created after the seconds irradiation.

4.3 Possibly made CNM

The results shown in section 3.8 will be discussed now. In summary, there are two unique data points:

1. Spot R: illuminated for 20 s by 75 eV electrons prior to annealing, directly after illumination, a front is observed. After all described annealing steps there is material left with a different structure (figure (23)).
2. Spot B: illuminated for 20 s by 20 eV electrons prior to annealing, no front was observed. After annealing this spot was indistinguishable from the substrate.

Possibly, the new structure observed on spot R after annealing could be cross-linked SAM or something close to graphene. *If* this were true, data suggests a link between the front and the cross-linking of BPT SAM. Presumably, the SAM structure was already altered after electron irradiation, which became visible after annealing. There is too little data to confirm a connection between the front and cross-linking, this requires more research. Later on we will provide some suggestions on how continue these investigations by use of AFM.

5. Conclusion

First we have demonstrated two working methods for the preparation of BPT SAMs. Then, LEEM has enabled us to do *in situ* observations on electron irradiation induced effects on BPT SAMs. These effects are seen as a collapsing ring, which we have referred to as a front. We conclude this front (i) to be more visible for either higher energy or longer illumination time and (ii) to start shrinking with a linear speed followed by a slight acceleration just before its disappearance. Furthermore, electron irradiation of BPT SAM by 75 eV electrons for 20 s at a size down to a 5 μm radius circle followed by annealing has yielded a new structure which - according to literature - should be cross-linked BPT SAM (i.e. CNM).

In conclusion, this preliminary research has shown many results from which most are still open for interpretation (e.g. UV-light induced effects on BPT SAMs, freezing of a front, disappearance of a frozen front, front speed dependence on electron energy and illumination time and a newly made structure upon electron irradiation of BPT SAM followed by annealing). LEEM is concluded to be an excellent technique to continue investigations, but should be combined with complementary techniques (e.g. spectroscopy, AFM, STM, etc.) to understand these results.

6. Outlook

Even though sublimation was chosen to be the better method for SAM fabrication, we believe that the method and used setup could be improved greatly. The used setup was made of glass and operated at pressures far above ultrahigh vacuum (10^{-9} mbar). Obviously, this leaves some room for improvements. One very interesting option would be to move sublimation to the ESCHER setup. This would allow the whole CNM fabrication process (substrate preparation²⁷, SAM sublimation and development through annealing) to be done *in situ*. Although the ESCHER setup cannot do CP-AFM measurements, we do not foresee this to be a major problem. Since CP-AFM measurements are merely a characterisation step, it would be safe to leave this step out once the SAM fabrication recipe is optimised and controlled.

The solution method could also be improved, which might lead to better results. It is advised to work extremely cleanly (e.g. cleaning all glassware with aggressive methods like Aqua Regia and purifying BPT by sublimation).

For this report, substrates which supposedly have a SAM on them were characterised by CP-AFM. However, this technique is unable to resolve whether the molecular layer is a true monolayer or a multilayer. Many of our interpretations assume that we have made monolayer. Therefore, further experiments are necessary to determine whether this assumption can be confirmed. By using spectroscopy techniques like XPS and ellipsometry a surface's chemical composition and layer depth can be measured.

It would be highly interesting to further investigate the 'addition rule' for illuminations. It is suggested to start with keeping the waiting time between subsequent illuminations (T_w) as short as possible, and start with only two exposures. Once this is understood, variation in T_w could reveal information of the 'memory time' of a SAM, i.e. how long does the surface 'remember' it was irradiated. Once a simple model is inferred, it could be falsified by more complex cases like three or more illumination steps.

We also recommend further research on the following question: could the new structure seen after irradiation and annealing be cross-linked BPT SAM and does seeing a front imply (partial) cross-linking? We sketch a simple experiment that could falsify the first question. In essence, one would like to redo the experiment but on a known location on the surface. After annealing, height information of this structure can be retrieved by scanning the location with AFM. *If* this structure indeed is cross-linked BPT SAM, one would expect to find a height difference between the substrate and newly made structure comparable to the length of a BPT molecule (≈ 10.7 Å). Regarding the second question, our data does not allow for any meaningful conclusion precisely because we illuminated either far above or below \mathcal{L} . To prove a connection between the front and cross-linking, it is advised should zoom in and illuminate spots with E_e , T_i close to \mathcal{L} .

A list of more things that might be interesting to look into for future research:

- Correlation between SAM age and front quality/speed. By measuring fronts on the same sample on subsequent days, a correlation might be found between SAM age and front visibility. This should qualitatively clarify how long a SAM can still be considered as good enough for experiments (given it is saved under certain conditions).
- Keep track of the LEEM electron gun current. Plots shown in this report regarding fronts show time on the horizontal axis where one would rather convert this to dose which is the more relevant quantity in this context. This can easily be done by formula (1) *if* the gun current is precisely known.
- Measuring E_t : we propose the threshold energy could be determined by illumination of BPT SAM in LEEM with long T_i and low E_e (say $\approx 1 - 2$ eV). However, the absence of a front for this measurement could be explained in two ways: (i) the electron energy used for illumination is

below the threshold energy, therefore, no front is seen. (ii) The rate of electron deposition is lower than the typical time-scale of the surface memory discussed above.

- In-between LEEM experiments, samples were stored in vacuum ($\approx 10^{-2}$ mbar). However, this does not keep a SAM from degrading over time (e.g. due to decreasing of the molecular surface density and accumulation of dirt on the SAM). Visibility of the front is believed to be correlated with the age of the SAM. Unfortunately, we cannot prove this with the present data set as there are too many varying parameters (e.g. made by different method).

Acknowledgements

I would like to thank my supervisors: Dr. ir. Sense Jan van der Molen, MSc Hüseyin Atesci and MSc Daniël Geelen. Their help, patience, enthusiasm and humour did not only help me in doing the research and writing this thesis, they also made it a very enjoyable experience.

(indicated by thick black lines) in nitrogen versus ambient atmosphere. Unless stated otherwise (number of days between brackets), substrates are immersed in a solution for three days. Likewise, sublimation is split by 4/24 hours. Four hour sublimations were always divided as two hours active and two hours without pumping. For 24 hour sublimation this division was not kept constant as indicated by the numbers between brackets (e.g. (7h, 17h) means 7h active and 17h no pumping). All attempts are numbered (1 to 18) by date (first try = 1, last try = 18). Furthermore some cells have a number in superscript, these numbers have the following meaning:

- 1: Sample is rinsed by DMF and ethanol *after* sublimation.
- 2: A chromium TEM grid was evaporated on top of gold substrate (measurements are done on gold).
- 3: Samples are placed standing up straight in solution during self-assembly.

It is important to note that the colour markings in this table are not objective. They depend on the used definition of 'good' CP-AFM data. A lower standard (e.g. allowing a wider spread in resistance), would result in more successful SAM fabrication attempts.

Appendix B

Our method to measure the position of a front (p_f) is now illustrated in a more mathematical way. It actually uses the centre of mass position of the arc (\mathcal{A}) clipped between a band of width w (see figure (B.1)). We will approximate the front to be circular for position measurements done along the short axis.

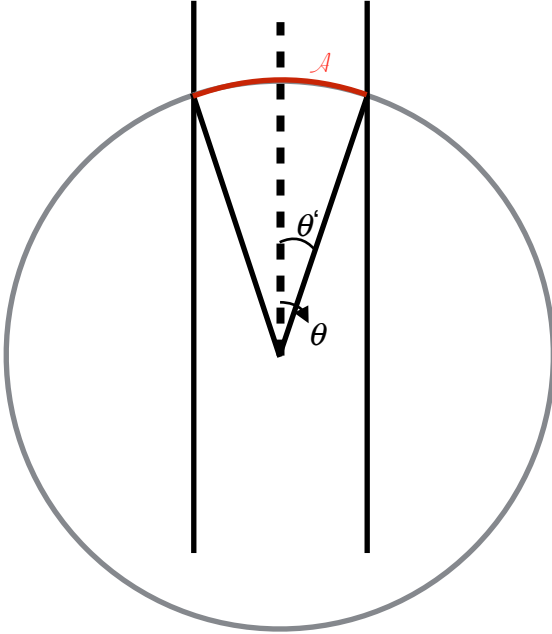


Figure B.1: A front of radius r is approximated by a circle. A part of the circle is clipped by a band of width w , this is \mathcal{A} (marked in red). The centre of mass of \mathcal{A} is calculated by integration using the polar angle as defined by θ .

We calculate p_f assuming a circular front of radius r for a given w . For each point on \mathcal{A} , we calculate the projection along the $\theta = 0$ direction, integrate this along \mathcal{A} and normalise by its total length.

$$p_f = \frac{\int_{\mathcal{A}} r \sin(\theta) r d\theta}{\int_{\mathcal{A}} r d\theta} = \frac{\int_{-\theta'}^{\theta'} r^2 \sin(\theta) d\theta}{\int_{-\theta'}^{\theta'} r d\theta} = \dots = \frac{w/2}{\arcsin(w/2r)}$$

Where we have used that (see figure (B.1)):

$$\theta' = \arcsin(w/2r)$$

We plot this function this result for $w = 30$:

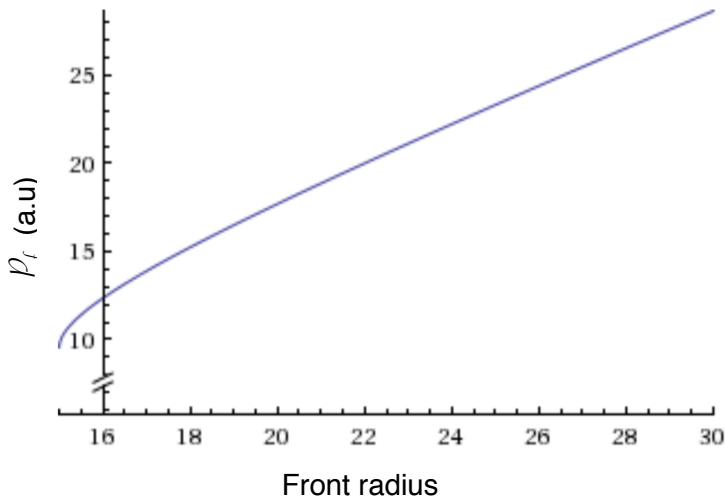


Figure B.2: Plot of the foregoing result for $w = 30$. The vertical axis shows the position of the front, as measured by the method described above. The horizontal axis shows the size of the front.

This illustrates that a front which is made to shrink linearly in time, is actually measured to accelerate towards the end if the method described above is used.

A more proper method would be to measure the front position as explained above, while keeping the *ratio* of enclosed arc length over w constant (instead of w). This means one should use a smaller w as the front shrinks. By doing so, the artificial acceleration that was introduced by the 'wrong' method is cancelled.

Reference list

1. Novoselov, K.S., Geim, A.K., Morozov, S.V., Jiang, D., Zhang, Y., Dubonos, S.V., Grigorieva, I.V., Firsov, A. A. Electric Field Effect in Atomically Thin Carbon Films.
2. Cooper, D. R. *et al.* Experimental Review of Graphene. *ISRN Condens. Matter Phys.* **2012**, 1–56 (2012).
3. Lee, C., Wei, X., Kysar, J. W. & Hone, J. Measurement of the elastic properties and intrinsic strength of Monolayer Graphene. **321**, 385–388 (2008).
4. Zhang, X., Beyer, A. & Götzhäuser, A. Mechanical characterization of carbon nanomembranes from self-assembled monolayers. *Beilstein J. Nanotechnol.* **2**, 826–833 (2011).
5. Turchanin, A. *et al.* Molecular mechanisms of electron-induced cross-linking in aromatic SAMs. *Langmuir* **25**, 7342–7352 (2009).
6. Zheng, Z. *et al.* Janus nanomembranes: A generic platform for chemistry in two dimensions. *Angew. Chemie - Int. Ed.* **49**, 8493–8497 (2010).
7. Nottbohm, C. T. *et al.* Novel carbon nanosheets as support for ultrahigh-resolution structural analysis of nanoparticles. *Ultramicroscopy* **108**, 885–892 (2008).
8. Striemer, C. C., Gaborski, T. R., McGrath, J. L. & Fauchet, P. M. Charge- and size-based separation of macromolecules using ultrathin silicon membranes. *Nature* **445**, 749–753 (2007).
9. Turchanin, A. *et al.* One nanometer thin carbon nanosheets with tunable conductivity and stiffness. *Adv. Mater.* **21**, 1233–1237 (2009).
10. Kumar, a & Whitesides, G. M. Patterned condensation figures as optical diffraction gratings. *Science* **263**, 60–62 (1994).
11. Beyer, A. *et al.* Fully cross-linked and chemically patterned self-assembled monolayers. *Phys. Chem. Chem. Phys.* **10**, 7233–7238 (2008).
12. Onclin, S., Ravoo, B. J. & Reinhoudt, D. N. Engineering silicon oxide surfaces using self-assembled monolayers. *Angew. Chemie - Int. Ed.* **44**, 6282–6304 (2005).
13. Aswal, D. K., Lenfant, S., Guerin, D., Yakhmi, J. V. & Vuillaume, D. Self assembled monolayers on silicon for molecular electronics. *Anal. Chim. Acta* **568**, 84–108 (2006).
14. Magnussen, O. M. *et al.* Self-assembly of organic films on a liquid metal. *Nature* **384**, 250–252 (1996).
15. Grönbeck, H., Curioni, A. & Andreoni, W. Thiols and disulfides on the Au(111) surface: The headgroup-gold interaction. *J. Am. Chem. Soc.* **122**, 3839–3842 (2000).
16. Schwartz, D. K. Mechanisms and Kinetics of Self-assembled Monolayer Formation. (2001).
17. Geyer, W. *et al.* Electron-induced crosslinking of aromatic self-assembled monolayers: Negative resists for nanolithography. *Appl. Phys. Lett.* **75**, 2401–2403 (1999).
18. Turchanin, A. *et al.* Fabrication of molecular nanotemplates in self-assembled monolayers by extreme-ultraviolet-induced chemical lithography. *Small* **3**, 2114–2119 (2007).

19. Zhang, X., Vieker, H., Beyer, A. & Götzhäuser, A. Fabrication of carbon nanomembranes by helium ion beam lithography. *Beilstein J. Nanotechnol.* **5**, 188–194 (2014).
20. Zharnikov, M., Geyer, W., Götzhäuser, a, Frey, S. & Grunze, M. Modification of alkanethiolate monolayers on Au-substrate by low energy electron irradiation: Alkyl chains and the S/Au interface. *Phys. Chem. Chem. Phys.* **1**, 3163–3171 (1999).
21. Angelova, P. *et al.* A universal scheme to convert aromatic molecular monolayers into functional carbon nanomembranes. *ACS Nano* **7**, 6489–6497 (2013).
22. Wold, D. J. & Frisbie, C. D. Formation of a Metal - Molecule - Metal Junction by Contacting an Alkanethiol Self-Assembled Monolayer with Formation of Metal - Molecule - Metal Tunnel Junctions : Microcontacts to Alkanethiol Monolayers with a Conducting AFM Tip. 2970–2971 (2000).
23. Tromp, R. M. *et al.* A new aberration-corrected, energy-filtered LEEM/PEEM instrument. I. Principles and design. *Ultramicroscopy* **110**, 852–861 (2010).
24. Kim, B., Choi, S. H., Zhu, X. Y. & Frisbie, C. D. Molecular tunnel junctions based on pi-conjugated oligoacene thiols and dithiols between Ag, Au, and Pt contacts: Effect of surface linking group and metal work function. *J. Am. Chem. Soc.* **133**, 19864–19877 (2011).
25. Ishida, T. *et al.* Electrical conduction of conjugated molecular SAMs studied by conductive atomic force microscopy. *J. Phys. Chem. B* **106**, 5886–5892 (2002).
26. Penner, P. *et al.* Charge Transport through Carbon Nanomembranes. (2014).
27. Kautz, J., Copel, M. W., Gordon, M. S., Tromp, R. M. & Van Der Molen, S. J. Titration of submonolayer Au growth on Si(111). *Phys. Rev. B - Condens. Matter Mater. Phys.* **89**, 1–6 (2014).